Heat Transfer through Calcium Carbonate-based Coating Structures: Observation and Model for a Thermal Fusing Process

Patrick A.C. Gane, Cathy J. Ridgway and J. Schoelkopf

Research and Development
Omya Development AG
CH-4665 Oftringen
Switzerland
patrick.gane@omya.com

Douglas J. Bousfield

University of Maine
Orono, Maine 04469-5737
USA
bousfld@maine.edu

ABSTRACT

An analysis of thermal conductivity through porous calcium carbonate-based coating structures is made to assist in many areas of coating and printing, such as toner fusing, heat set offset, paper coating and finishing, including drying and calendering, and to support the recent studies into the potential for dry coating methods. Properties of coatings applied in the dry state have been shown in many respects to be able to match those conventionally produced using water-based formulations. There remains, however, in all these processes a need to understand the various fusing steps, in the case of dry coating for internal cohesion and adhesion of the coating to the paper surface, and the design and operation of the system, and in the case of thermal toner adhesion for the application and spatial control of thermal gradients. A method is developed to measure the thermal conductivity of a coating structure directly, and the coefficient of thermal conductivity is reported for several pigment/binder combinations, including a unique latex coated pigment in which the polymer latex binder is distributed in a thin film over the pigment surface. By modelling the pore structures using a network simulator, it is shown that connectivity in cases of inhomogeneous species distribution, such when both pigments and binders are present, is a necessary but not complete descriptor of thermal conductivity. It is shown that the heat conduction at similar skeletal connectivity is strongly dependent on the distribution of polymeric binder: the more uniform the binder distribution the greater is the thermal conductivity. A heat transfer model is described that can be used to predict the thermal transfer via conduction and, hence, simulate thermal processes including the fusing step.

Keywords: thermal properties of porous media, thermal conductivity of coatings, pigmented coatings, thermal fusing, heat set conductivity, dry coating, coating fusing, high temperature calendering.

INTRODUCTION

The thermal conductivity properties of porous media depend predominantly on the constituents present in the material making up the solid phase or skeleton of the structure. In the case of dry, or nearly dry, coatings, these materials consist of pigments and binder(s), the relative distribution of each defining the conductive contacts between the skeletal elements of the structure. Both the latter stages of drying and calendering of coatings rely on the thermal transfer properties of the coating layer in relation to the substrate and to the mechanical deformation properties of the layer composite. Furthermore, the application of the paper as a substrate for many printing processes including traditional heat set web offset techniques, as well as digital toner adhesion and fusion properties, requires a better understanding of the thermal transfer and conductive properties of the coating surfaces used.

In recent years, the potential of dry coating has been investigated. Both in open references, by Maijala *et al*. and Putkisto *et al*. [1-8], and in internal work it has been shown that the coating structures developed by dry coating methods approximate well to the pore structure distributions of wet applied coatings. The better the dispersion of the binder and pigment in the formulation mix, the better is the match with wet coating. The industrial research authors of this paper have been active in developing an optimal system for the pigment and binder, applicable in many coating application forms including both wet and dry methods, in which the binder (natural or synthetic, such as polymer latex) is distributed as a thin film over the surface of calcium carbonate. This material has been included in the series of experiments performed and reported here, and compared with 100 % calcium carbonate pigment alone and with formed and dried mixes of calcium carbonate and latex. The potential for such materials extends beyond the sphere of new coating application methods and may contribute to improved printing properties, especially where the control of thermal conductivity is critical.

To provide macroscopic samples for thermal gradient and capacity testing, tablets of coating structures have been formed and characterised by mercury porosimetry, following the methods described by Gane *et al.* and Schoelkopf *et al*. [9,10]. A method has been developed at the University of Maine, Orono, to measure the thermal transfer coefficient of the porous tablet structures using a transient experimental method. Different formulation coatings display different heat transfer coefficients, but all have similar heat capacities. A model is developed to interpret the experimental data. The model is also modified to predict the temperature distribution in a coating during and after a fusing step. Predictions seem reasonable and demonstrate large differences between coatings.

The porous structures of the tablets have been modelled using the network simulator Pore-Cor[1] such that any correlation between the heat transfer coefficients of the tablets and their purely structural properties can be investigated and compared with the

[1] Pore-Cor is a software developed by the Environmental and Fluid Modelling Group, University of Plymouth, Devon, PL4 8AA, U.K.

distribution effects of binder and pigment on thermal conductivity within the skeletal structure.

EXPERIMENTAL

Materials

The following formulations were used to make tablets for this analysis:

A - non dispersed chemical-free 75 wt% < 1 μm calcium carbonate mixed with styrene acrylic-based polymer latex in the weight ratio 100:10
B – polyacrylate dispersed 75 wt% < 1 μm calcium carbonate mixed with styrene acrylic-based latex in the weight ratio 100:10
C – polyacrylate dispersed 75 wt% < 1 μm calcium carbonate alone
D - speciality pigment consisting of styrene acrylic latex-coated 75 wt% < 1 μm calcium carbonate also in the weight ratio of 100:10

Tablet Formation

The tablets made from formulations A, B, C and D were formed in a special filtration apparatus by applying a constant pressure (*P*) of 0.5 MPa, for the undispersed samples A and D, and 1.5 MPa, for the deflocculated samples B and C, to the respective suspension/slurry for up to 1 hour, such that water was released by filtration through a fine 0.025 μm filter membrane resulting in a compacted tablet of the pigment or pigment latex combination. The apparatus used is shown schematically in Figure 1.

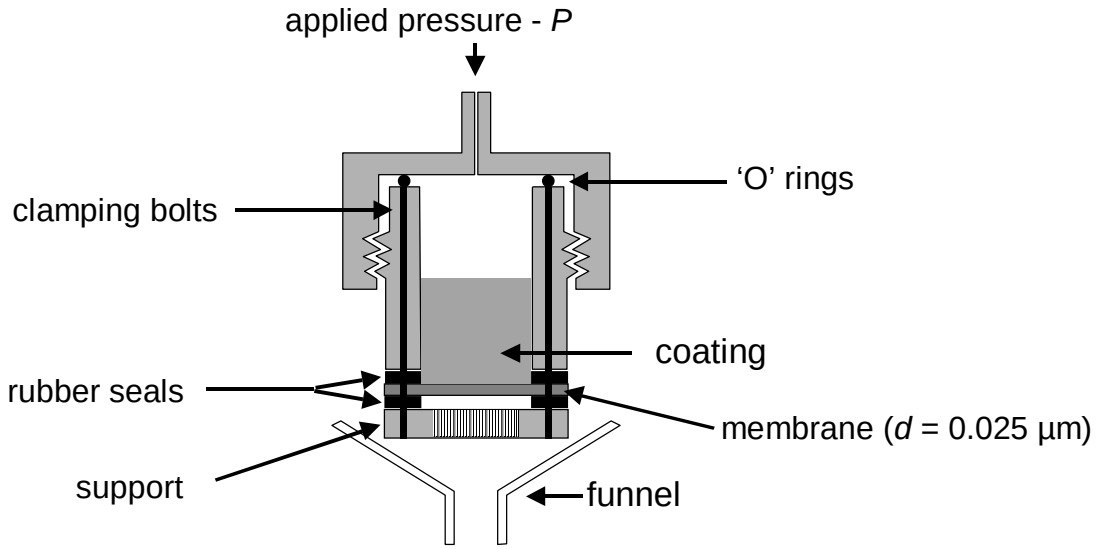

Figure 1 Apparatus designed for making tablets from wet suspensions (after, for example, [10]).

The tablet was removed from the apparatus and dried in an oven at 60 ^{o}C for 24 hours. This method produces tablets of ~ 4 cm diameter with a thickness of 1.5 – 2.0 cm, which can be sectioned and fashioned into suitable sample configurations for subsequent analysis.

Tablets made from A, B and D shrank somewhat on drying. Previous analysis has shown that tablets made this way, despite shrinking on drying, do have homogeneous internal structures. Samples were, therefore, taken from the interior of the tablets.

SEM images of the surfaces of the tablets are shown in Figure 2. Visually there seems to be very little difference between the structures.

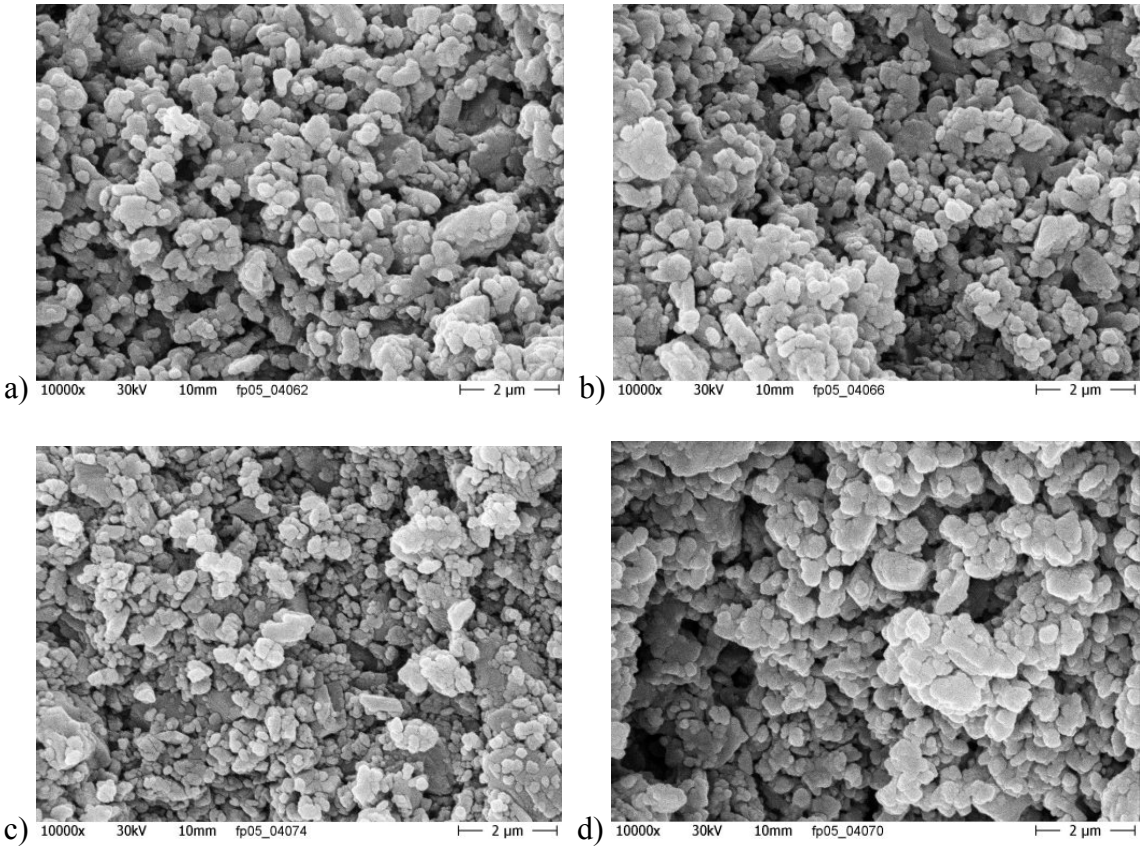

Figure 2 SEM images of the freshly cleaved surfaces of the tablets formed from formulations a) A, b) B, c) C and d) D

A more detailed schematic image of the pigment latex mixes, derived from an image analysis study of transmission electron microscope images using latex staining with osmium tetroxide, is given in Figure 3, in which the dark particles represent the latex and the white areas represent the calcium carbonate pigment. Some coalescence is observed, but the particle form of the latex in these examples remains intact.

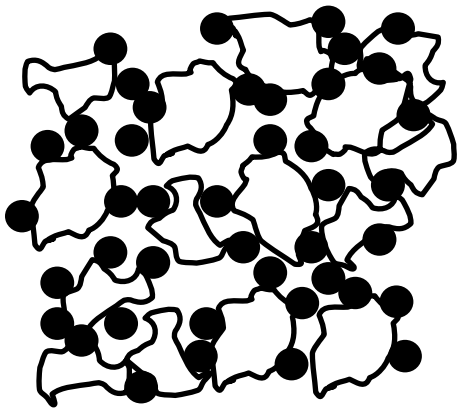

Figure 3 Schematic image of slurry product plus latex mix as seen in Tablet A – the black dots are latex particles and the bright particles are calcium carbonate particles.

In distinct contrast, particles from pigment Tablet D are shown, also schematically, in Figure 4. The image illustrates the unique proximity of the binder layer to the pigment surface, in which the latex is covering the carbonate and forms a film-like structure on the mineral surface.

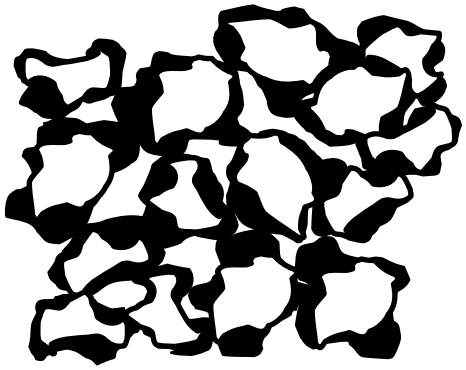

Figure 4 Schematic image of pigment D, in which the latex is covering the pigment surface in the form of a film, following the principles of formation of pigment-binder for dry coating.

Mercury Porosimetry

A portion of each tablet block is characterised by mercury porosimetry for both porosity and pore size distribution using a Micromeritics Autopore IV mercury porosimeter. The maximum applied pressure of mercury was 414 MPa, equivalent to a Laplace throat diameter of 0.004 μm (~ nm). The mercury intrusion measurements were corrected for the compression of mercury, expansion of the penetrometer and, where appropriate, the

compression of the solid phase of the sample using the equation of Gane *et al.* [9], employed in the software Pore-Comp[2].

Figure 5 shows the intrusion curves after the Pore-Comp correction.

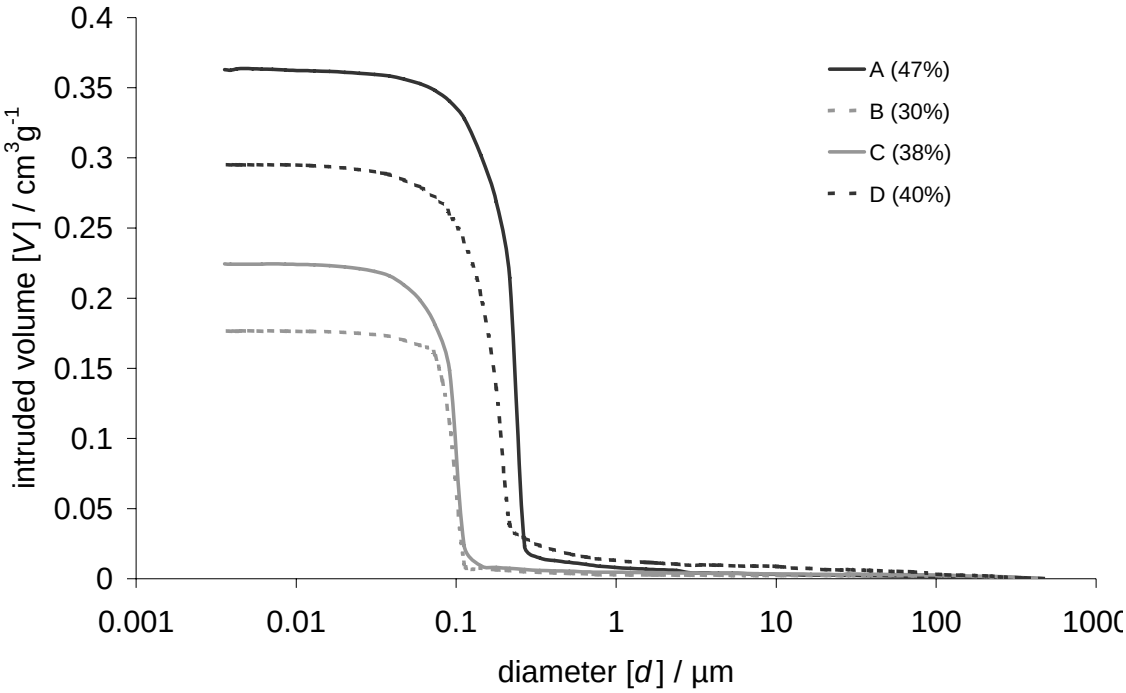

Figure 5 Mercury intrusion curves – porosity shown in brackets.

The porosity given by this method is representative of the pore space available to the mercury up to the highest applied pressure. The porosity values are given in the legend of Figure 5.

It is traditional to look at the first derivative of the cumulative mercury intrusion curves to find a representative void size distribution – Figure 6. This, however, takes no account of pore shielding (an effect where the non-wetting mercury needs to break through a small constriction to enter a larger feature) and represents in effect a simple bundle of capillary tubes. However, to describe the available individual space sizes in the tablets it is a useful first approximation.

[2] Pore-Comp is a software name used by the Environmental and Fluid Modelling Group, University of Plymouth, PL4 8AA, U.K.

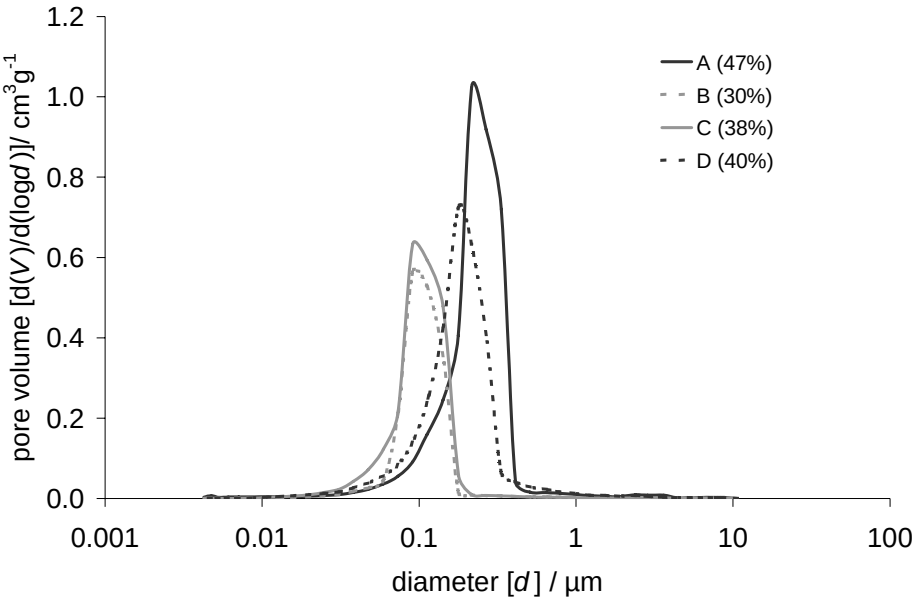

Figure 6 First derivative of mercury intrusion curves for the tablets, showing the equivalent capillary pore size volume distributions.

Tablets B and C have similar pore size distributions with the peak at 0.01 µm. Tablet B is constituted from the same dispersed pigment as Tablet C, but the addition of polymer latex in B is seen to act to fill some of the pores at ~ 0.10 - 0.15 µm, thus giving a lower total intruded volume, as seen in Figure 5. The latex size is itself ~ 0.14 µm.

Tablet A is made from an undispersed pigment, and, therefore, exhibits a degree of flocculation. These flocs lead to larger pores, the peak in the pore size distribution being at 0.22 µm, and, hence, a more porous structure, as can be seen by the intruded volume in Figure 5. The pore size distribution peak for Tablet D lies between the other samples with the peak at 0.18 µm.

Heat Capacity and Transfer Test

The heat capacities of the samples were measured with a standard method. The samples where heated to a uniform temperature, then placed in a known volume of water (of known heat capacity) held in an insulating calorimeter (also of known heat capacity). The change in water temperature was recorded. Table 1 contains the heat capacities. As expected, the heat capacities are nearly the same because the tablets are made of similar materials and dominated by calcium carbonate in weight terms.

A heat transfer test method has been developed. In this test, a MIRAK 4-Place Stirrer and Stirring Hot Plate, from the Barnstead International Co. (Model No.: SP 73325-60), is used as the steady heat source to heat the tablet under investigation. An OMEGA HH12 Digital Thermometer (Dual Input Model with Type K Thermocouple Input) is used to

measure the temperature of the bottom and the top of the tablet. The data indicated by the digital thermometer are accurate to the nearest whole degree.

A round hole has been made in a square-shaped foam. In the experiment, as shown in Figure 7, the tablet is put into the hole. The foam acts as a layer of insulation. A cotton ring is put around the tablet to prevent the air from circulating within the gap between the foam and the tablet. One temperature sensor is put on the top of the tablet. Another temperature sensor is put between the tablet and the heating plate. Both sensors are connected to the digital thermometer. A single foam lid is put on the top of the sensor and the tablet as an insulating layer. Ambient humidity conditions are assumed, such that heating is made slowly enough to allow equilibrium within the tablet to be established.

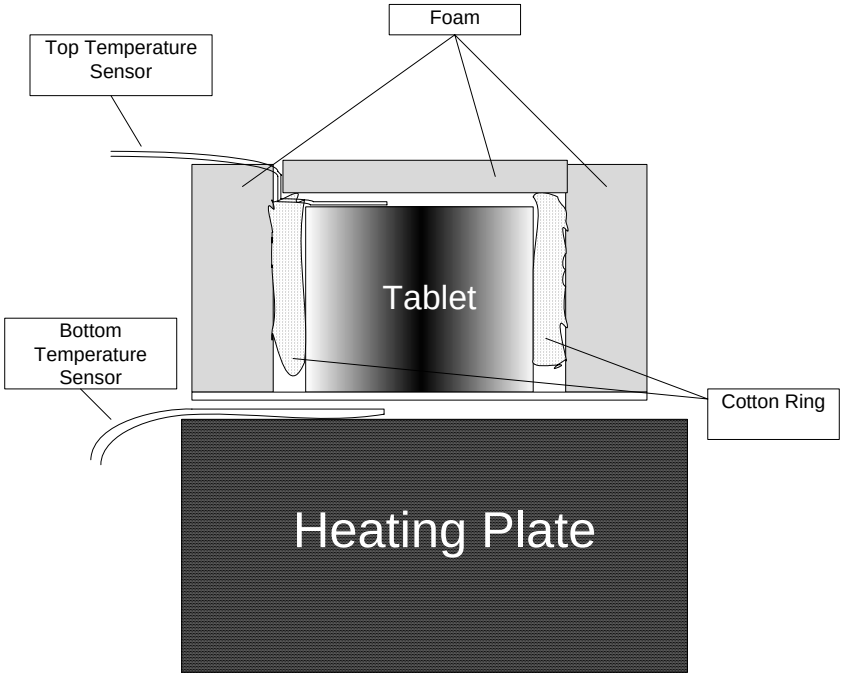

Figure 7 Heat transfer experiment.

Eight tablets have been tested at three heating temperatures: 50 ^{o}C, 70 ^{o}C and 90 ^{o}C each tablet material being tested twice in separate samplings. No visual property changes in the tablets were observed during or after the heating tests.

Dimensions of the tested tablets are shown in the Table 1. The data shown in the table are the average of four measurements made each on two tablets to illustrate reproducibility.

Table 1 Tablet dimensions, porosity and thermal properties

	Diameter /mm	Height /mm	Porosity /%	Heat capacity /cal $g^{-1o}C^{-1}$	Heat capacity /J $kg^{-1o}C^{-1}$	Thermal conductivity /$Js^{-1}m^{-1o}C^{-1}$
A1	29.91	13.74				0.10
A2	29.20	12.71	47	0.13	543	0.11
B1	36.75	13.09				0.12
B2	38.86	12.22	30	0.14	585	0.13
C1	35.13	18.58				0.05
C2	36.92	12.93	38	0.12	501	0.08
D4	29.61	11.96				0.14
D5	27.42	8.08	40	0.13	543	0.24

Figures 8-19 show the raw data as temperature against time as measured from the bottom and top of the sample, respectively. The temperature near the heat source (bottom) jumps up to the applied temperature as expected. The temperature on the other side of the tablet (top) increases gradually over time to a level near that of the bottom surface. Due to some inevitable heat loss through the sample side, the top surface does not reach the temperature of the heated surface. However, this is not a problem because the dynamic heat transfer is the important issue.

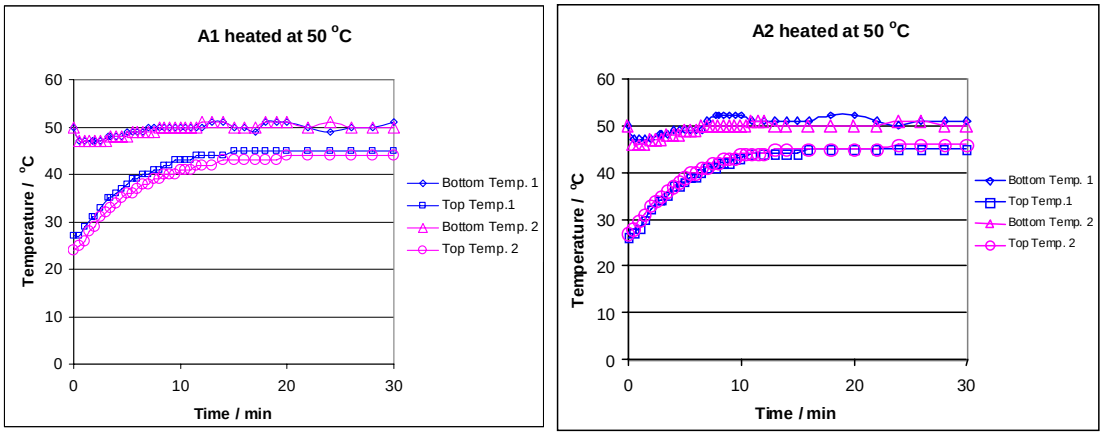

Figure 8 Sample A1 and A2 heated to 50 °C.

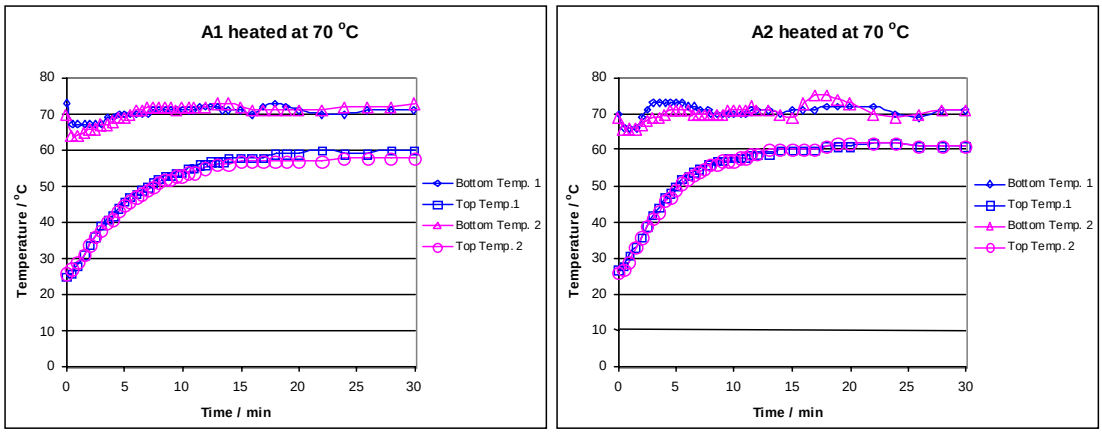

Figure 9 Sample A1 and A2 heated to 70 °C.

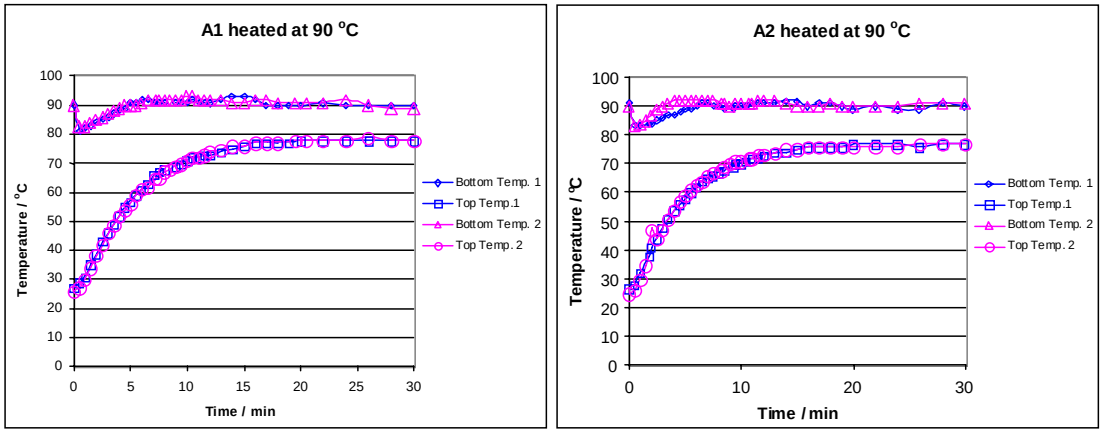

Figure 10 Sample A1 and A2 heated to 90 °C.

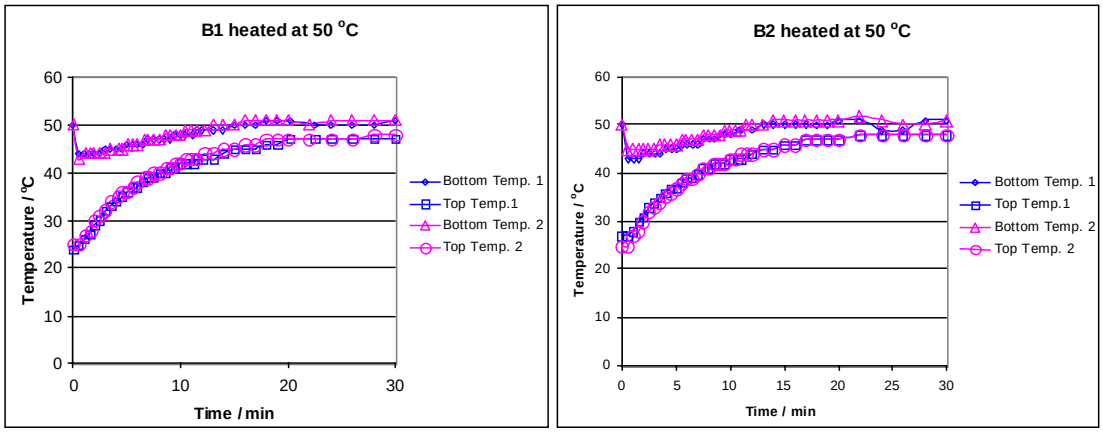

Figure 11 Sample B1 and B2 heated to 50 °C.

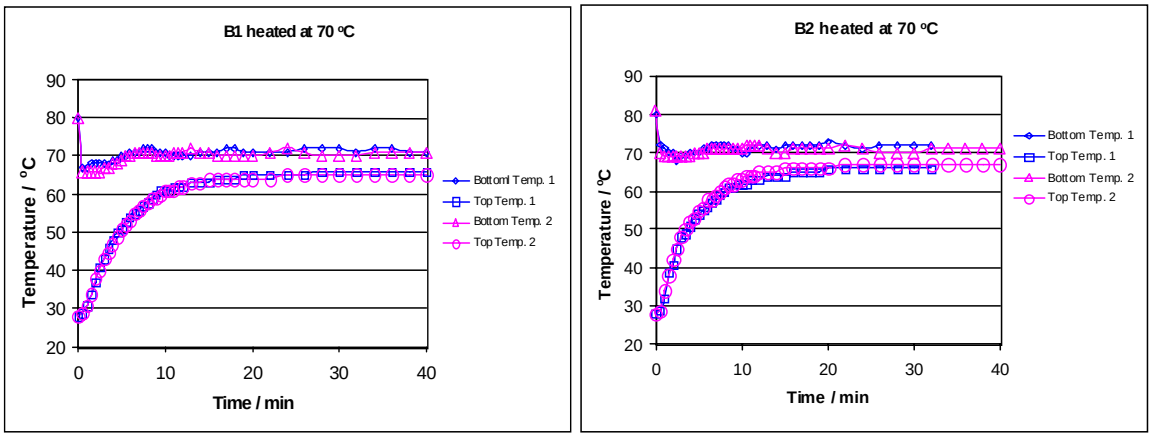

Figure 12 Sample B1 and B2 heated to 70 °C.

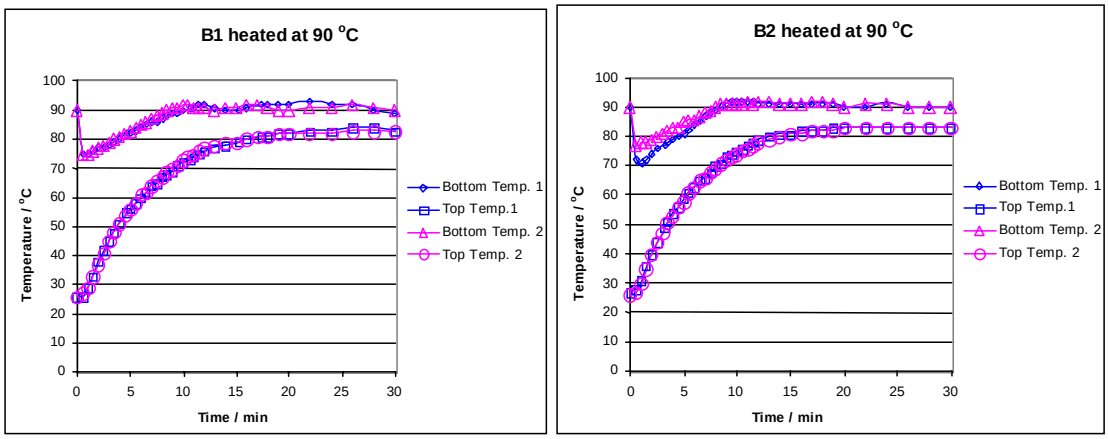

Figure 13 Sample B1 and B2 heated to 90 °C.

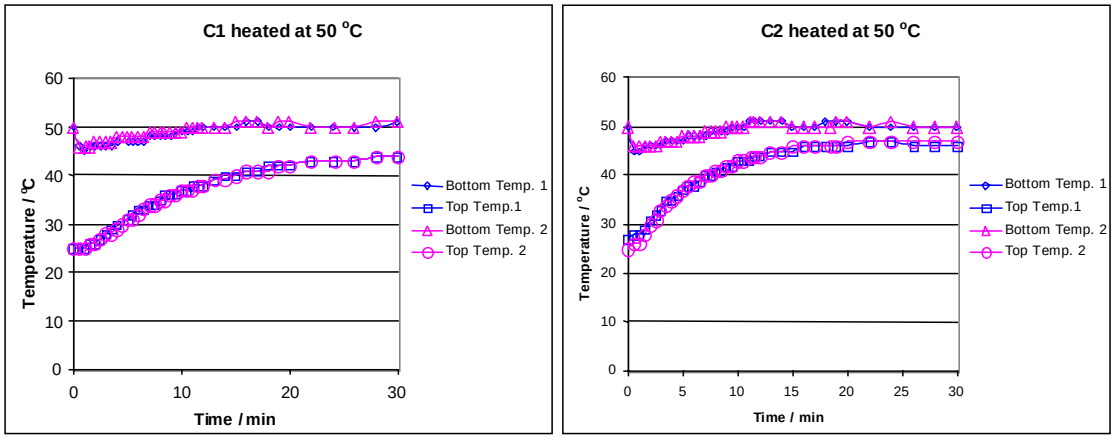

Figure 14 Sample C1 and C2 heated to 50 °C.

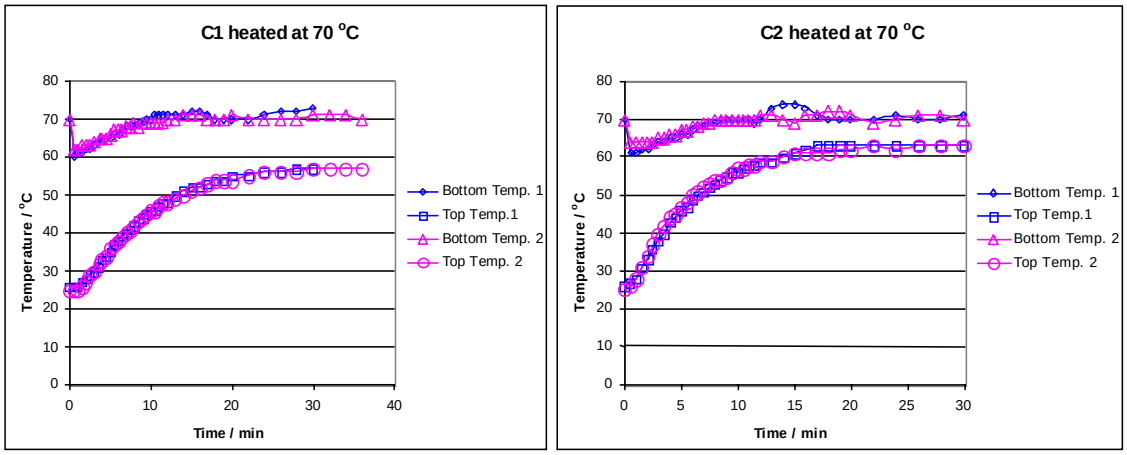

Figure 15 Sample C1 and C2 heated to 70 °C.

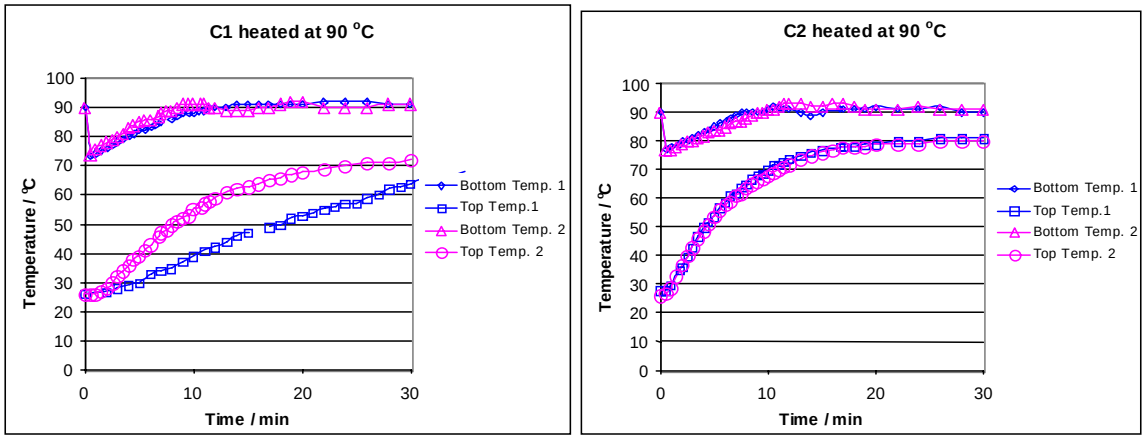

Figure 16 Sample C1 and C2 heated to 90 °C.

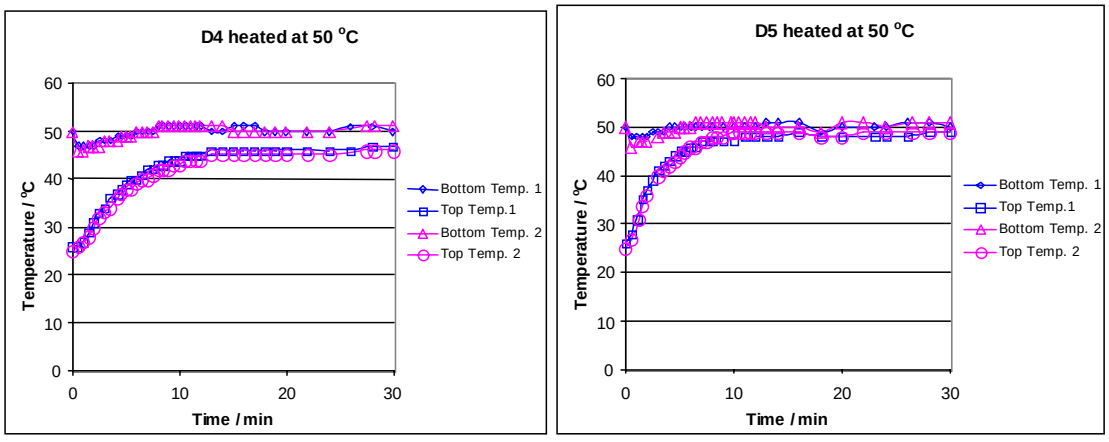

Figure 17 Sample D4 and D5 heated to 50 °C.

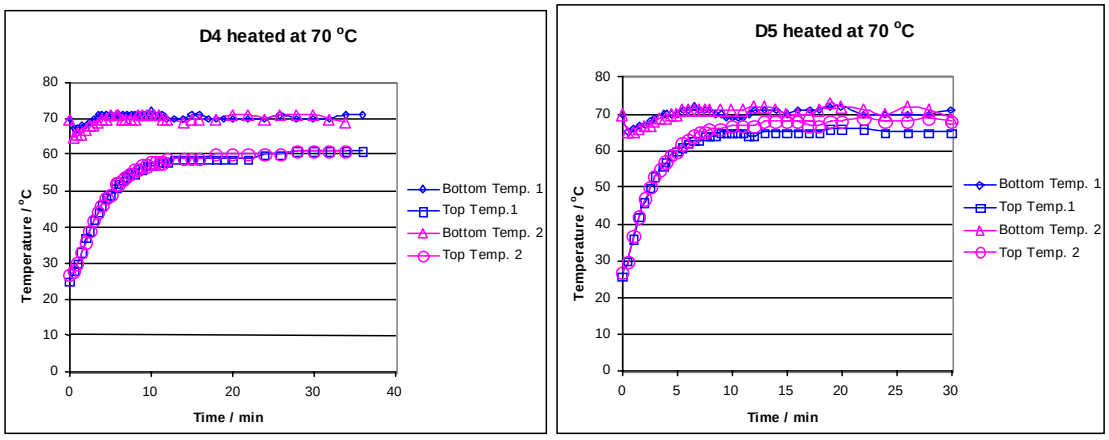

Figure 18 Sample D4 and D5 heated to 70 °C.

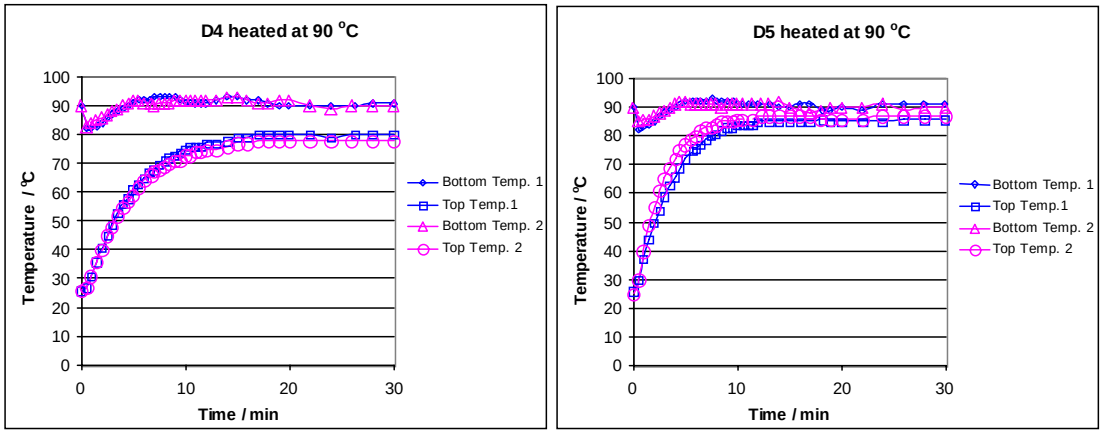

Figure 19 Sample D4 and D5 heated to 90 °C.

There are clear differences between the samples, but reproducibility for a given sample type is excellent. In all cases, sample D seems to respond quickly to the temperature and reaches a plateau at around seven minutes. Sample A and B seem to be intermediate. Sample C is slower. Since they have similar porosity, it is unlikely that porosity per se is controlling the thermal conductivity. Even without considering heat capacity issues, we would assume that sample D has a high heat transfer coefficient while sample C has a low value. In light of the similar heat capacities shown in Table 1, we see that this expectation is indeed correct

THEORY

The rate of heat transfer along the axis of a cylinder is well established, and derivable from Fourier's Law of heat conduction [16]. These experiments are dynamic. Therefore,

a time dependent problem must be solved. An energy balance on a differential slice of the cylinder leads to the following differential equation:

$$\rho C_p \frac{\partial T}{\partial t} = k \frac{\partial^2 T}{\partial z^2} - 2\frac{h}{R}(T - T_a) \tag{1}$$

where ρ is the density of the material, C_p is the heat capacity, T and T_a are temperatures of the material at any position and the ambient air, respectively, k is the thermal conductivity, h is the heat transfer coefficient, and R is the radius of the cylinder. Figure 20 shows a depiction of the situation. One assumption is that the temperature of the material is constant in the radial direction.

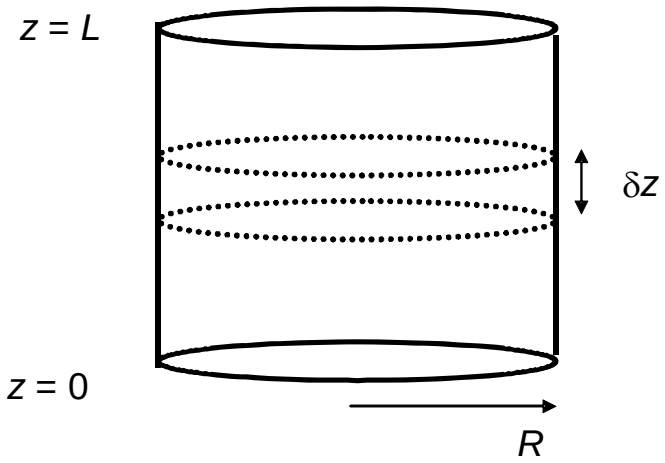

Figure 20 Geometry of the heat transfer problem.

The initial condition is that the material is all at some ambient temperature T_a. The boundary conditions are an applied temperature at $z = 0$ and a no flux condition at $z = L$. The equation is solved with standard finite difference methods with a FORTRAN code.

If Eq. (1) is divided through by the density and heat capacity, the term $k/\rho C_p = D$ is often called the thermal diffusivity. Figure 21 shows the result of the temperature at the top of a small tablet when the bottom is set at 50 ^{o}C for two different reduced heat transfer coefficients. When the loss to the sides is zero, the top surface will approach the bottom temperature. When the loss is finite, the top temperature never reaches that of the bottom, because energy is lost through the sides of the cylinder.

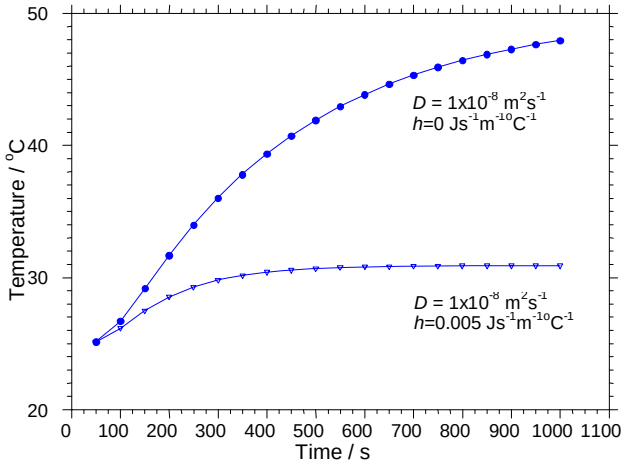

Figure 21 Temperature at the top of the tablet for two different heat transfer coefficients.

The temperature profile through the axial position in the tablet is shown in Figure 22. At short times, the temperature increases only near the bottom of the cylinder. As time increases, the top temperature increases. If the heat loss to the sides is zero, the cylinder will become a uniform temperature equal to the bottom temperature.

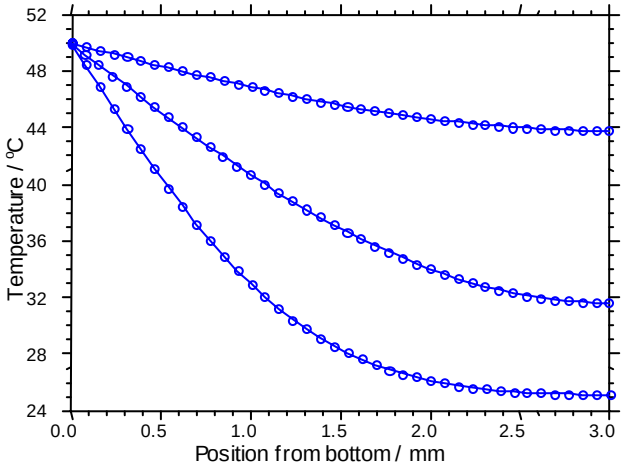

Figure 22 Temperature profile in cylinder when bottom is held at 50 °C.

The influence of different thermal diffusivities is as expected: as the diffusivity increases, the rate of increase of the temperature at the top of the cylinder increases.

Match to Experiments

Two parameters in the model are adjusted to match the measured temperature response. The heat transfer coefficient between the tablet and the insulation controls the final temperature of the top surface. A high value reduces the result. This parameter, though, is not of main interest. The thermal diffusivity is adjusted to match the dynamic response, and this is the parameter of greater interest. Figure 23 shows the predicted temperature result that should match the conditions in Figure 8.

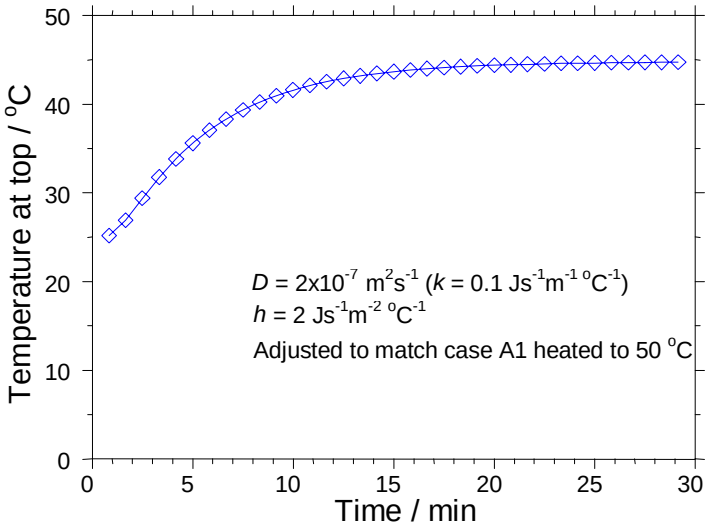

Figure 23 Predicted temperature increase of the top surface of the tablet for the case in Figure 8, Tablet A heated at 50 °C.

Using the same thermal diffusivity, and looking at the 90 °C case, Figure 24 shows the prediction. The heat transfer coefficient had to be adjusted a bit, maybe because the tablet was packed a bit differently in the device, but the dynamics are well predicted with the same value of thermal conductivity as in Fig. 23. The temperature response is about 5 % lower than the measured values, but considering the number of assumptions, the results can be considered as excellent. The predicted results for 70 °C case are also good, shown in Figure 25.

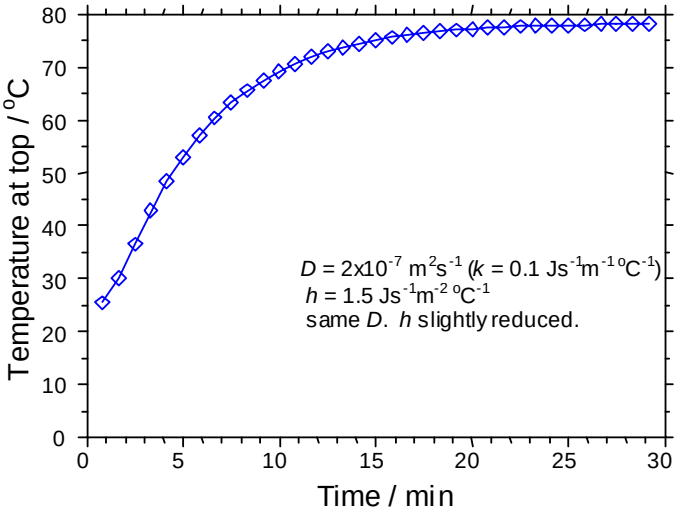

Figure 24 Predicted temperature response for case A1 heated to 90 °C, as compared to Figure 10.

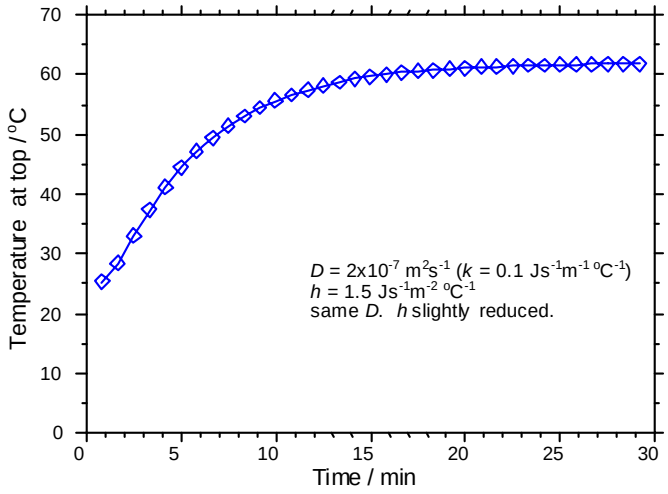

Figure 25 Predicted temperature response for case A1 heated to 70 °C, compared to Figure 9 - no adjusted parameters.

The values of the thermal conductivity needed to fit the data for the samples are those given in Table 1. Clearly, sample D5 has the highest values and sample C1 has the lowest. The technique to characterise this thermal conductivity parameter is, therefore, established.

In all other cases, the results at 90 °C were used to determine thermal conductivity, but the model could also predict the behaviour of the other two temperatures.

MODELLING THE STRUCTURE USING THE NETWORK SIMULATOR

Connectivity

The tablet structures have been replicated using a network computer model, which simulates the void-space structure of porous materials. The model has been employed previously to illustrate structures of a wide range of porous materials including sandstones [11], medicinal tablets [12] and soil [13]. It uses a unit cell with 1 000 cubic pores in a 10x10x10 array, connected by up to 3 000 throats, i.e. one connected to each cube face, that are either cylindrical or double conical [14] according to the prevailing geometry of the sample material. The structures are optimised such that the simulated intrusion curves match as closely as possible the experimental mercury intrusion curves, and the experimental porosity is accurately reproduced.

The model provides not only a structure that eliminates the effects of pore shielding by considering the porosity in combination with the given Laplace pressures, but also delivers a representative connectivity, allowing this parameter to be studied in the context of thermal conductivity. A further feature is the ability to describe zones of varying structure when a simple logarithmic pore size distribution of randomly placed pores fails to achieve a satisfactory match with experiment [15]**.**

The network simulator can be used to gain further insight into the pore structure of the tablets. The simulated intrusion curves match closely the experimental mercury intrusion curves, Figure 26, and the experimental porosity is accurately reproduced. The unit cell for sample C is shown in Figure 27.

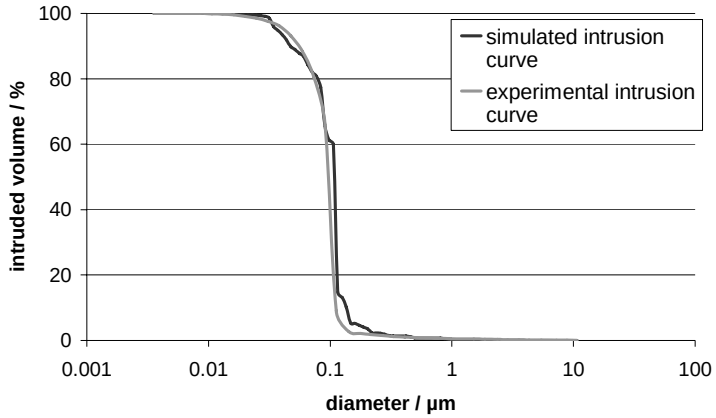

Figure 26 Simulated and experimental mercury intrusion curves for sample C.

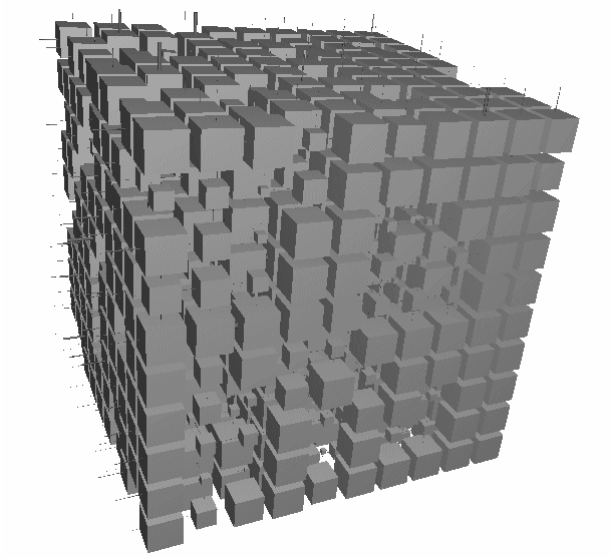

Figure 27 Simulated network structure using cylindrical throats for sample C, unit cell size = 133.35 μm.

The parameters for the simulated structures for the four tablets are shown in Table 2 below.

Table 2 Network model parameters for the modelled structures.

	min. diam. / μm	max. diam. / μm	throat skew	connectivity	pore skew	correlation level and unit cell type	porosity / %	unit cell size / μm
Tablet A	0.004	10.69	1.60	4.56	115.58	0.06 vertical banding	47	135.11
Tablet B	0.004	10.69	2.49	5.31	77.56	0.20 vertical banding	30	144.29
Tablet C	0.004	10.69	2.49	5.31	77.56	0.20 vertical banding	38	133.35
Tablet D	0.004	10.69	2.00	5.00	200.00	random	40	143.06

Tablet D has been shown to have the highest values of heat conductivity and Tablet C the lowest. By comparing the structural parameters, for example connectivity, it is clear to see that there is no direct correlation between heat conductivity and structural parameters alone. In these cases, the connectivity is very similar, with perhaps sample A having the least, and, since the thermal conduction is made via the skeletal material and not by the voids, connectivity could be expected to be an important parameter. However in this analysis it seems that connectivity is a necessary but not complete descriptor of conductivity.

We now go on to analyse whether permeability may be a controlling factor.

Simulated Permeability

The continuous flow, or permeability, can be expressed in terms of the Darcy permeability constant, k, using Darcy's Law, [17], in which a volumetric flow rate q through the sample, length l, cross sectional area A, containing a fluid of viscosity η, flowing under a differential pressure ΔP is expressed as:

$$q = \frac{\mathrm{d}V}{\mathrm{d}t} = k\frac{A\,\Delta P}{\eta\, l} \tag{2}$$

The laminar flow resulting in a parabolic velocity distribution within a liquid volume V, in time t, for a horizontal circular tube of length l, radius r, containing a fluid of viscosity η, flowing under a differential pressure ΔP, is expressed via the Poiseuille equation as:

$$\frac{\mathrm{d}V}{\mathrm{d}t} = \frac{\pi r^4 \Delta P}{8\eta\, l} \tag{3}$$

where the term r^4/l corresponds to the volumetric flow capacity Ξ. In using the Poiseuille equation, it should be recognised that it is only a first approximation to the resistive flow of a feature within the network.

Now it is assumed that Poiseuille flow occurs across the whole cell:

$$\left(\frac{\mathrm{d}V}{\mathrm{d}t}\right)_{\text{cell}} = -\frac{\pi}{8\eta}\,\Omega_{\text{cell}}\left(\Xi_{\text{arcs}}\right)\Delta P_{\text{cell}} \tag{4}$$

where $\underset{\text{cell}}{\Omega}$ is an averaging operator over the whole unit cell, as described in the work of [18] operating on the flow capacities of the arcs (Ξ_{arcs}) in which an arc represents a pore-throat-pore pathway between nodes sited at the centre of each pore. Each arc in the flow network is the flow channel between adjacent nodes, positioned at the centre of each pore. It generates a term which is related to the effective Poiseuillean capacity of the cell for flow in the $-z$ direction (from the top to the bottom face), and in the $\pm x$ and $\pm y$ direction. Flow, however, is not allowed in the $+z$ direction, thereby applying an implicit positive pressure gradient with respect to z. A network analysis approach to this problem supplies a term $\underset{\text{cell}}{\Omega}(\Xi_{\text{arcs}})$ as the maximal flow capacity through the network of pores and throats. It is calculated by means of the 'Dinic' network analysis algorithm [18]. There is an overall conservation of flow, so that the entire volume of fluid entering the top of the unit cell emerges at the bottom, with no build-up through the network. The value obtained, as the maximal flow, is an average of the capacity values over only those channels found to carry flow.

The combination of the Poiseuille equation, Eq. (3), with the Darcy equation, Eq. (2), results in an expression for the absolute permeability independent of the pressure gradient imposed on the sample:

$$k = \frac{\pi}{8} \underset{\text{cell}}{\Omega} \left(\Xi_{\text{arcs}} \right) \frac{l_{\text{cell}}}{A_{\text{cell}}} \tag{5}$$

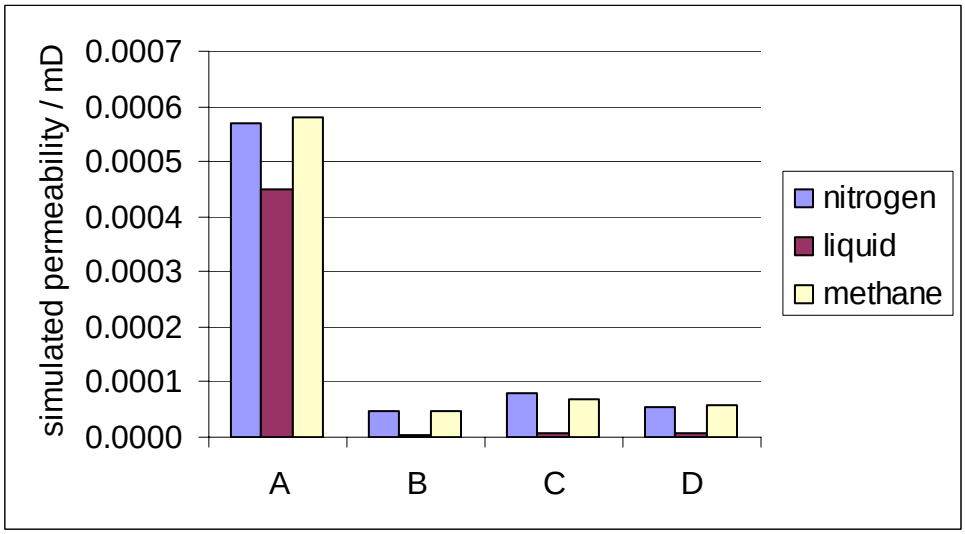

Figure 28 Network simulated permeabilities.

Figure 28 shows the modelled permeabilities, given in milliDarcies, of the samples for one typical liquid and two gases. These permeability values reflect the much more porous and open structure of the flocculated undispersed pigment used in Tablet A. Other than

this major difference, the permeability of the other samples is very similar, and follows the similarity in connectivity. This is not surprising, since the skeletal particle sizes are very similar except in the case of Tablet A (same pigment particle size except for the flocculated structure A), and so permeability is a likely resultant of the connectivity alone in samples B, C and D. It is clear to see, therefore, that the thermal conductivity is not related directly to the permeability of the simulated structures. However, the concept of the permeability dependence on connectivity and pore size is supported.

Given the independence of thermal conductivity in this series from direct relation with the individual structural parameters of the samples, we must deduce that thermal conductivity is in these cases related to the species distribution in the material.

THERMAL CONDUCTIVITY MODEL PREDICTIONS

Now that the thermal conductivity can be measured, the temperature distribution in a coating layer during a fusing step can be predicted. The two main factors are the role of temperature and the dwell time or time of contact. The same equation as given in Eq. (1) can be solved now to predict the temperature profiles.

For a coating layer of 20 μm, and a roll surface temperature of 150 ^{o}C, the final temperature profiles at different contact times are shown in Figures 29 and 30 using the thermal conductivities of coatings C and D, respectively. For coating C, a contact time of around 5 ms is needed to increase the temperature of the coating near the fibres to over 100 ^{o}C. For coating D, only 1 ms is needed. There is clearly quite a difference in behaviour between these coatings depending on their thermal conductivity.

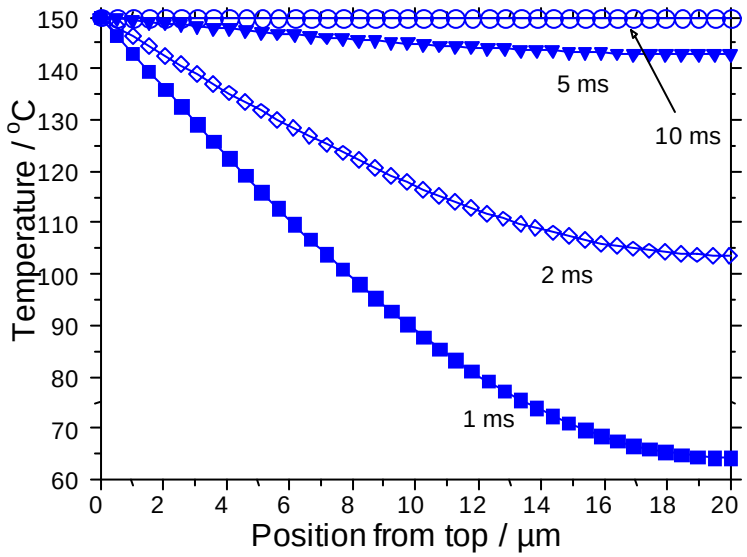

Figure 29 Predicted temperature profiles in coating layer for coating C1 at different contact times with a theoretical roll temperature of 150 ^{o}C.

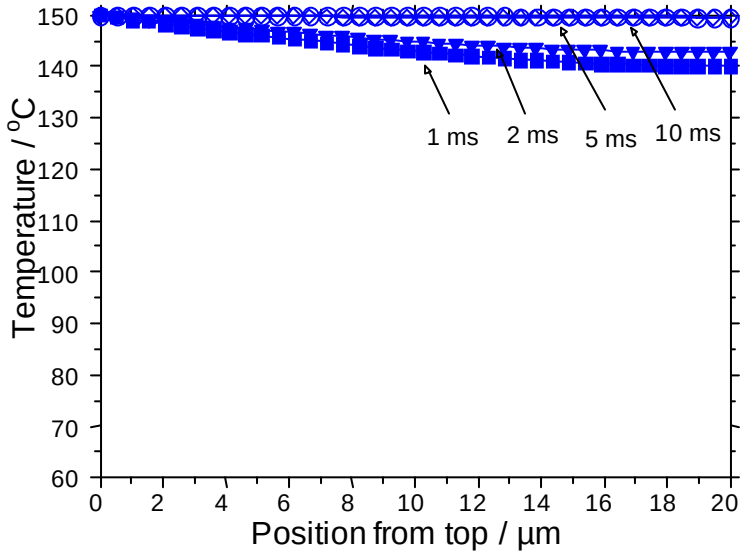

Figure 30 Predicted temperature profiles in coating layer for coating D5 at different contact times with a theoretical roll temperature of 150 °C.

SUMMARY AND CONCLUSIONS

A method to measure the thermal conductivity of porous structures has been developed. The method is applicable to pigmented coating structures and adopts the heat transfer properties of a macroscopic tablet of coating. By use of a code to solve the dynamic heat transfer equation, the thermal conductivity can be determined. The value at one temperature is seen to be quite good in predicting the behaviour at other temperatures.

Four structures were studied, including undispersed, flocculated, and dispersed pigment with and without latex, and these were compared with a specially-designed pigment which has latex distributed on its surface.

The tablet containing only dispersed calcium carbonate pigment showed the lowest thermal conductivity, whereas the tablet made from the latex coated pigment showed the greatest thermal conductivity. The SEM images of the two tablets show the pore structures to be very similar. Two other samples, containing undispersed and dispersed pigment, respectively, both with latex added separately, showed thermal conductivities lying between these two extremes, despite the strong flocculation of the undispersed sample leading to significantly higher porosity.

By modelling all the structures, using a computer network simulator, more detailed structural parameters could be considered. It is seen that connectivity is a necessary but

not complete descriptor of thermal conductivity when comparing samples with and without latex. The thermal conductivity behaviour does not track with permeability either, which was shown to differ even though connectivity remained similar. In fact permeability is a complex combination of pore size and connectivity. Therefore, it is concluded that the thermal conductivity is not dependent directly on the pore structure of the tablets, provided they have similar connectivity, but rather on their components and their respective spatial distributions. The pigment coated with latex exhibits the most intimate component contact, whereas pigment alone, despite similar connectivity, is latex free. The continuous contact of latex throughout the tablet results in the faster thermal conductivity. The other samples, also containing latex, do not form continuous polymer contact in the same way as in the speciality case.

The thermal conductivity model was shown to be suitable to predict the temperature increase in the coating layer during a finishing or fusing step.

A number of further improvements could be made to the model, but this work represents a first step to understand the thermal transfer properties of a paper coating and hence its impact on such factors as finishing, binding strength and during fusing.

REFERENCES

1. Maijala, J., Putkisto, K. and Grön, J., "*Coating layer formation in dry surface treatment of paper substrates*", TAPPI J., 3(5):20, 2004

2. Putkisto, K., Maijala, J., Grön, J. and Rigdahl, M. "*Preparation of coating particles for dry surface treatment of paper - the effects of particle aggregation on coating structure*", Nordic Pulp and Paper Res. J., 18(2):226, 2003

3. Putkisto, K., Maijala, J., Grön, J. and Rigdahl, M., "*Influence of the binder thermomechanical properties on the fixing process and structure of dry surface treated papers*", J. Pulp and Paper Sci., 30(6):145, 2004

4. Putkisto, K., Maijala, J., Grön, J. and Rigdahl, M., "*Viscoeleastic properties of the polymer binder affecting processability, structure and properties of dry surface treated papers*", TAPPI J., 3(6):19, 2004

5. Maijala, J., Putkisto, K. and Grön, J., "*Effect of coating powder composition and process conditions on surface structure and ink interactions of dry surface treated papers*", Wochenblatt für Papierfabrikation, Professional Papermaking, 1:84, 2004

6. Putkisto, K., Maijala, J., Grön, J. and Rigdahl, M., "*An approach to the dry-state preparation of coating particles for use in dry surface treatment of paper*", Progr. Org. Coatings, 51(4):257, 2004

7. Putkisto, K., Maijala, J., Grön, J. and Rigdahl, M., "*Polymer coating of paper using dry surface treatment: Coating structure and performance*", TAPPI J., 3(11):16, 2004

8. Putkisto, K., Maijala, J., Grön, J. and Rigdahl, M., "*Challenges set for coating powders applied to dry surface treatment of paper*", Paper presented at the 9th Tappi Coating Fundamentals Symposium, 8-10 February 2006, Åbo Akademi University, Turku, Finland, TAPPI PRESS pp19-27

9. Gane, P. A. C., Kettle, J. P., Matthews, G. P. and Ridgway, C. J., "*Void space structure of compressible polymer spheres and consolidated calcium carbonate paper-coating formulations*", Industrial and Engineering Chemistry Research, 35(5), 1996, p1753-1764

10. Schoelkopf, J., Gane, P.A.C. and Ridgway C.J., "*Observed non-linearity of Darcy-permeability in compacted fine pigment structures*", Colloids and Surfaces A, Physicochem. Eng. Aspects, 2004, vol 236/1-3 pp 111-120

11. Matthews, G. P., Ridgway, C. J. and Small, J. S., "*Modelling of simulated clay precipitation within reservoir sandstones*", Marine and Petroleum Geology, 13(5), 1996, p581-589

12. Ridgway, C. J., Ridgway, K. and Matthews, G. P., "*Modelling of the void space of tablets compacted over a range of pressures*", Journal of Pharmacy and Pharmacology, 49, 1997, p377-383

13. Peat, D. M. W., Matthews, G. P., Worsfold, P. J. and Jarvis, S. C., "*Simulation of water retention and hydraulic conductivity in soil using a three-dimensional network*", European Journal of Soil Science, (March 2000), 2000, p65-79

14. Ridgway, C. J., Schoelkopf, J., Matthews, G. P., Gane, P. A. C. and James, P. W., "*The effects of void geometry and contact angle on the absorption of liquids into porous calcium carbonate structures*", Journal of Colloid and Interface Science, 239(2), 2001, p417-431

15. Matthews, G. P., Moss, A. K. and Ridgway, C. J., "*The effects of correlated networks on mercury intrusion simulations and permeabilities of sandstone and other porous media*", Powder Technology, 83(1), 1995, p61-77

16. Bird, R. B., Stewart, W. E., and Lightfoot, E. N., "*Transport Phenomena*", Wiley, New York, 2002, p850

17. Darcy, H., 1856, "*Les Fontaines publiques de la Ville de Dijon, Libraire des corps imperiaux des ports et chaussees et des mines, Paris*"

18. Matthews, G. P., Moss, A. K., Spearing, M. C. and Voland, F., "*Network calculation of mercury intrusion and absolute permeability in sandstone and other porous media*", Powder Technology, (76), 1993, p95-107

Heat Transfer through Calcium Carbonate-based Coating Structures: Observation and Model for a Thermal Fusing Process

Patrick A.C. Gane

Omya

1865 THE UNIVERSITY OF MAINE

Fusing processes

- Digital printing
  - Laser toner adhesion
  - Wax and thermal setting inks
- Heatset web offset
  - Evaporation of ink components
  - Reduction of viscosity for absorption
  - Thermally-induced polymerisation
- Coating processes
  - Wet coating (blade, filmpress, spray, curtain…….)
    - Drying process
    - Calendering
      - Role of latex binder
  - Dry Coating [for example, Maijala *et al*. and Putkisto *et al*. (2004)]
    - Polymer-pigment constructions
    - Fusing internally and to the basepaper

Materials

- **A:** non-dispersed (chemical-free)
  - 75 wt% < 1 μm $CaCO_3$
  - + 10 parts added styrene acrylic-based latex binder
- **B:** polyacrylate dispersed
  - 75 wt% < 1 μm $CaCO_3$
  - + 10 parts added styrene acrylic-based latex binder
- **C:** polyacrylate dispersed
  - 75 wt% < 1 μm $CaCO_3$ only
- **D:** speciality self-binding pigment
  - styrene acrylic ***latex-coated*** 75 wt% < 1 μm $CaCO_3$
    - (= 10 parts latex)

Tablet formation

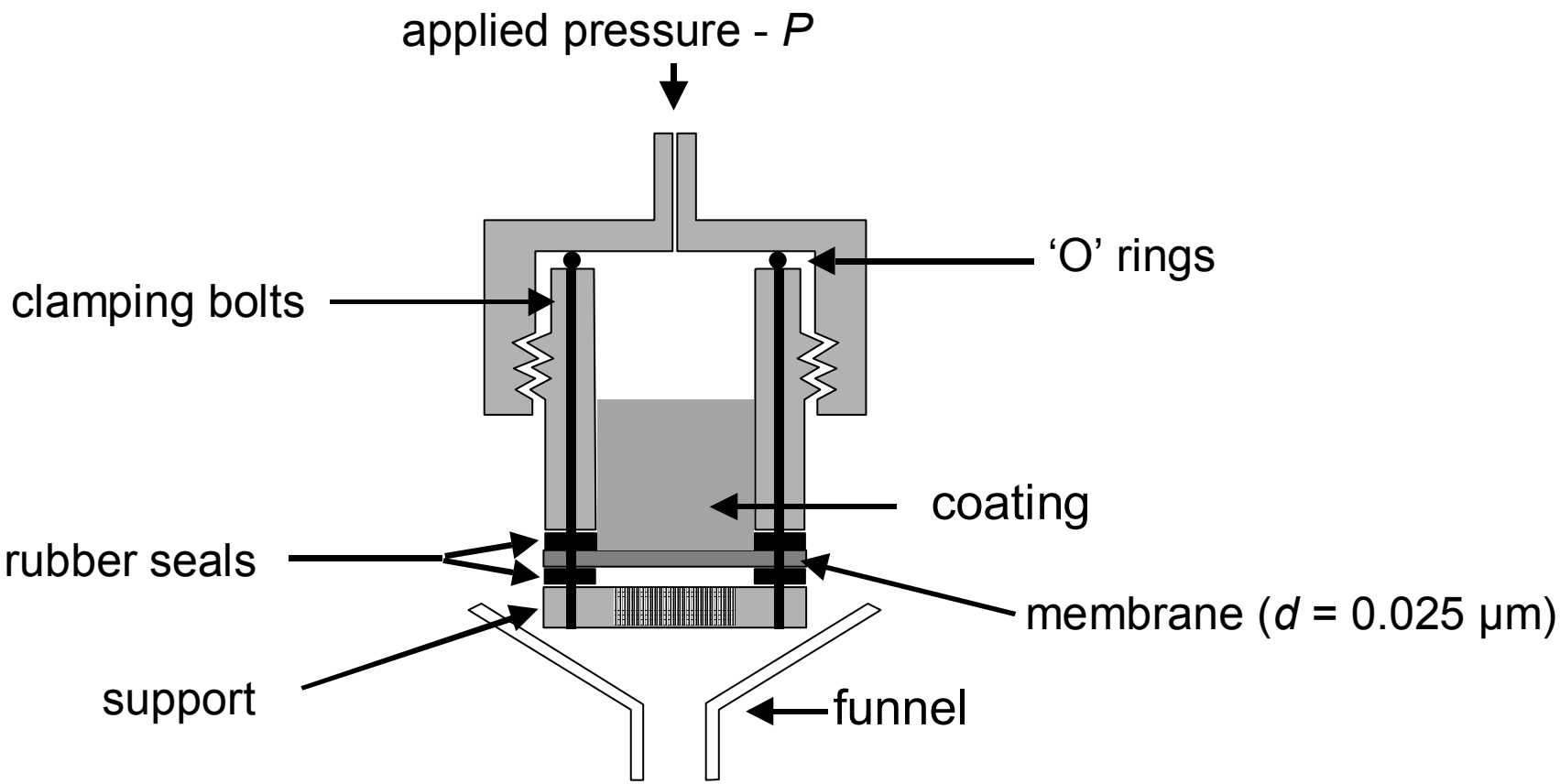

[Schölkopf *et al*. (2004)]

Pigment Tablets

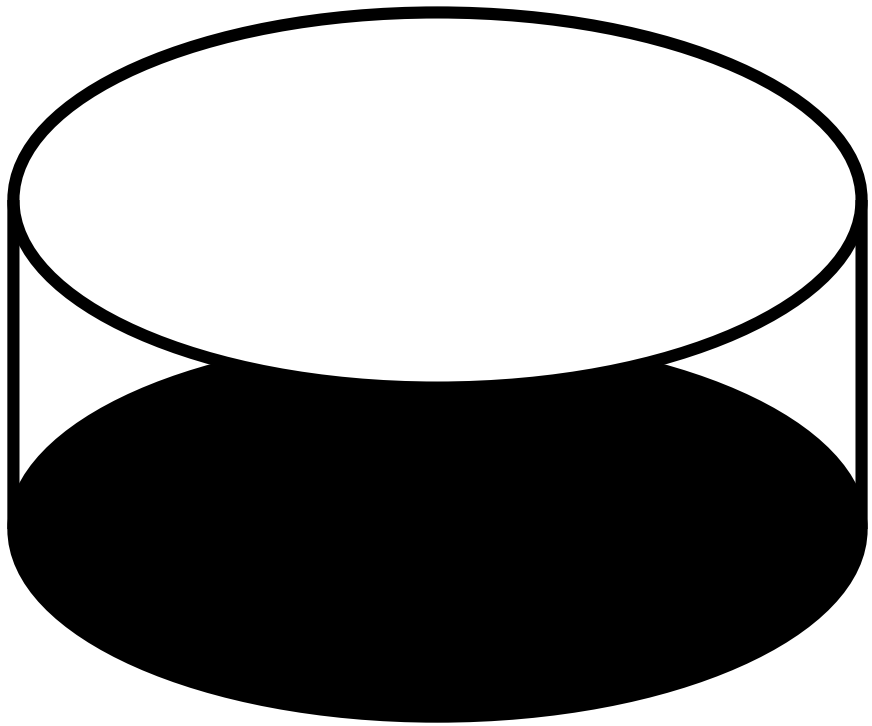

SEM view of the structures

A

non-dispersed mix

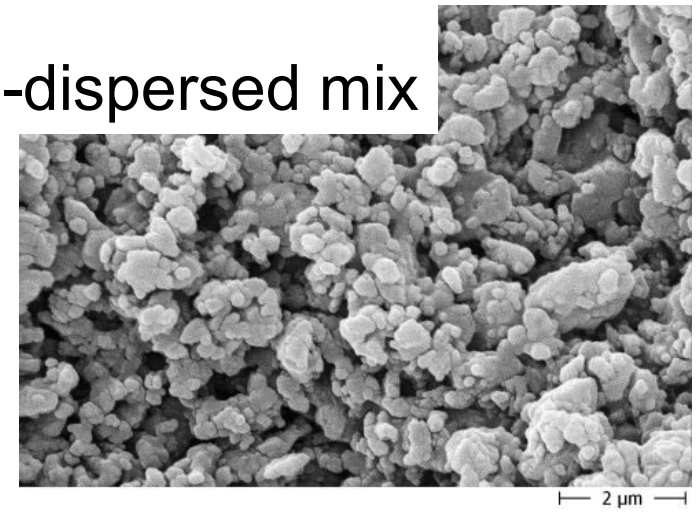

B

dispersed mix

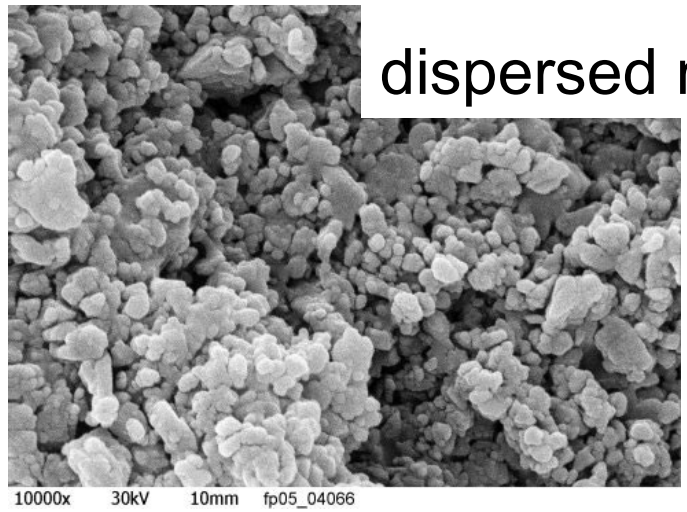

C

non-dispersed $CaCO_3$

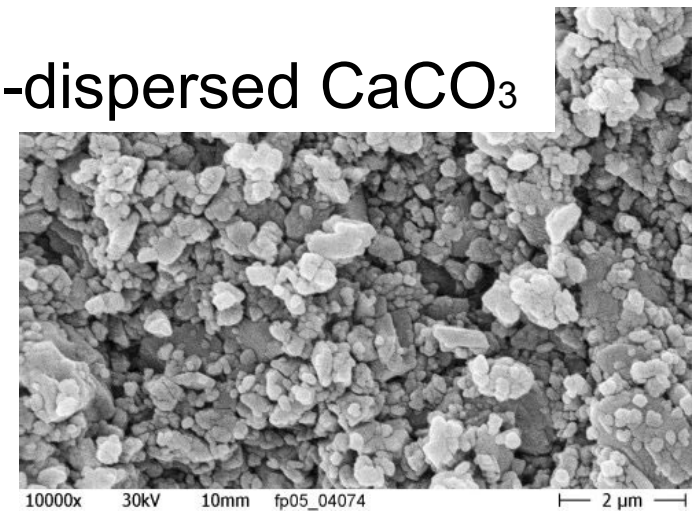

D

speciality

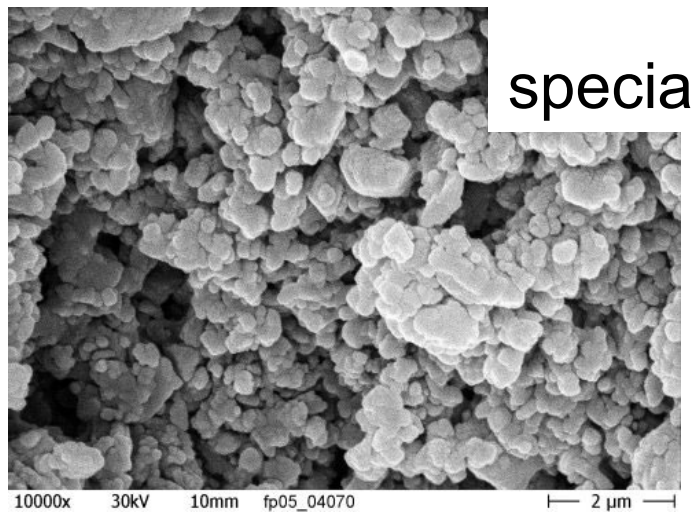

Mix versus Speciality

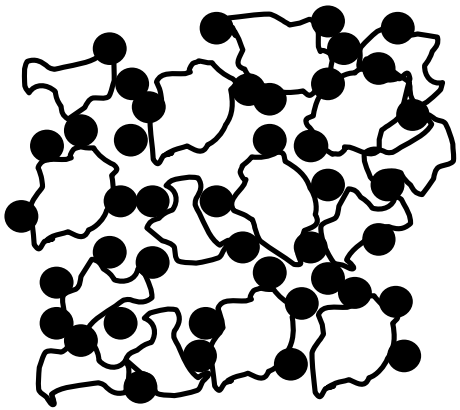

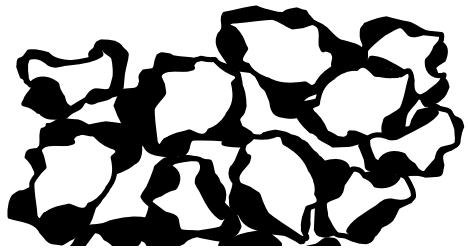

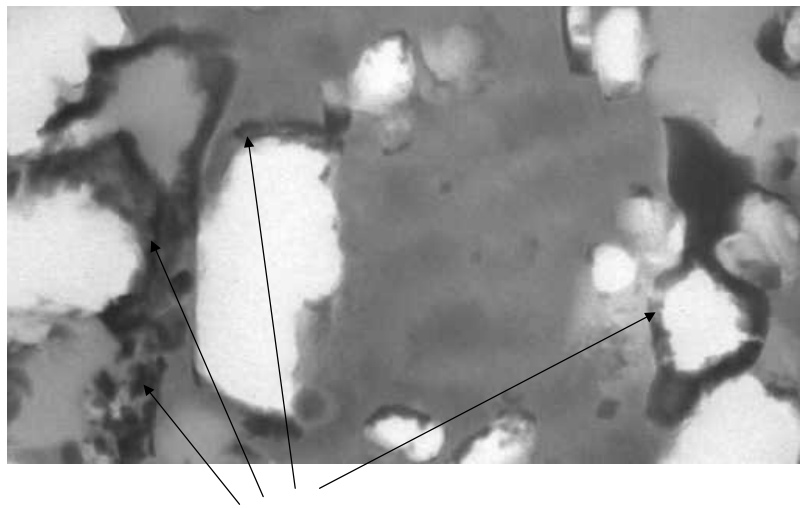

Latex layer on the particles

Thermal Capacity and Conductivity

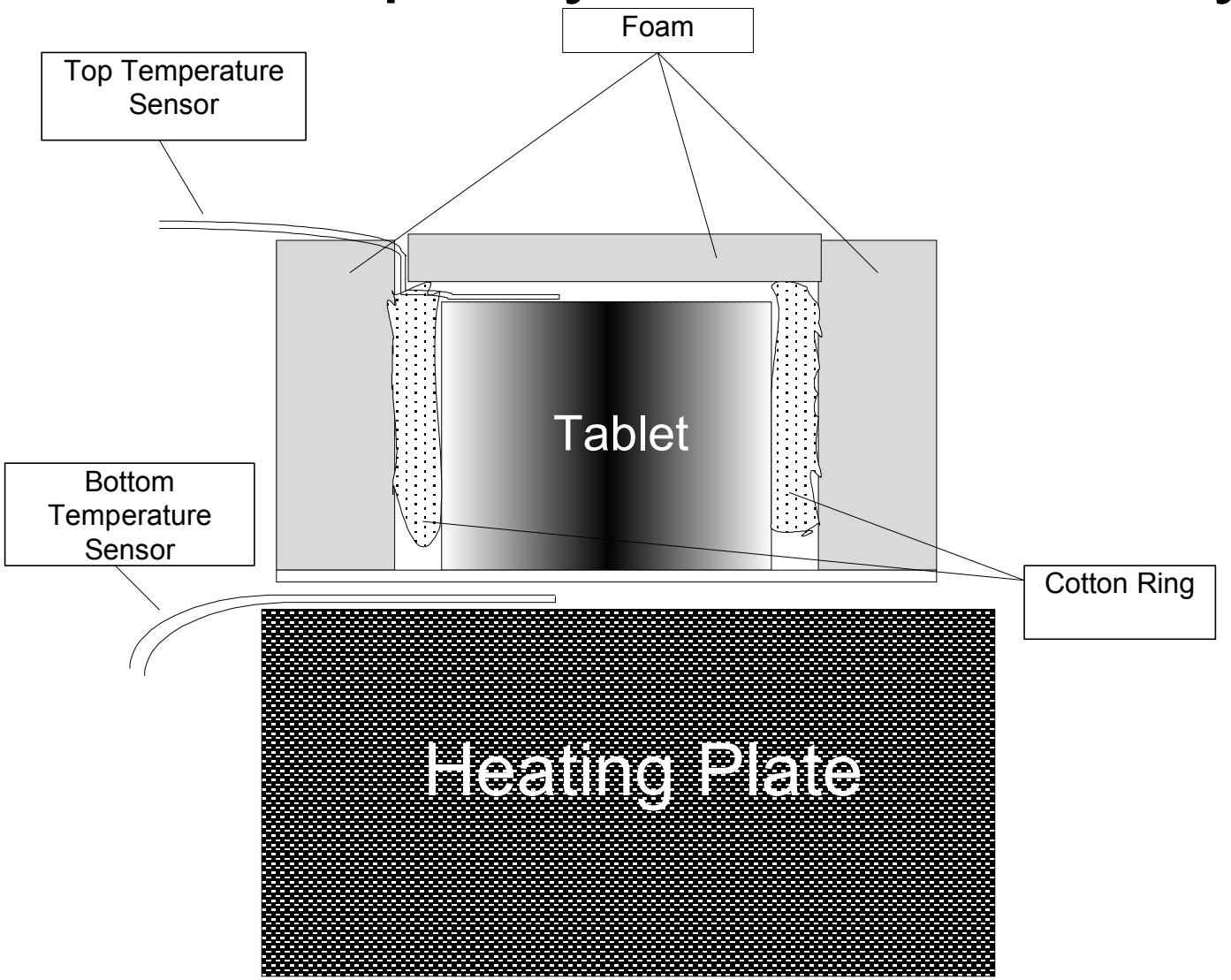

Reproducibility

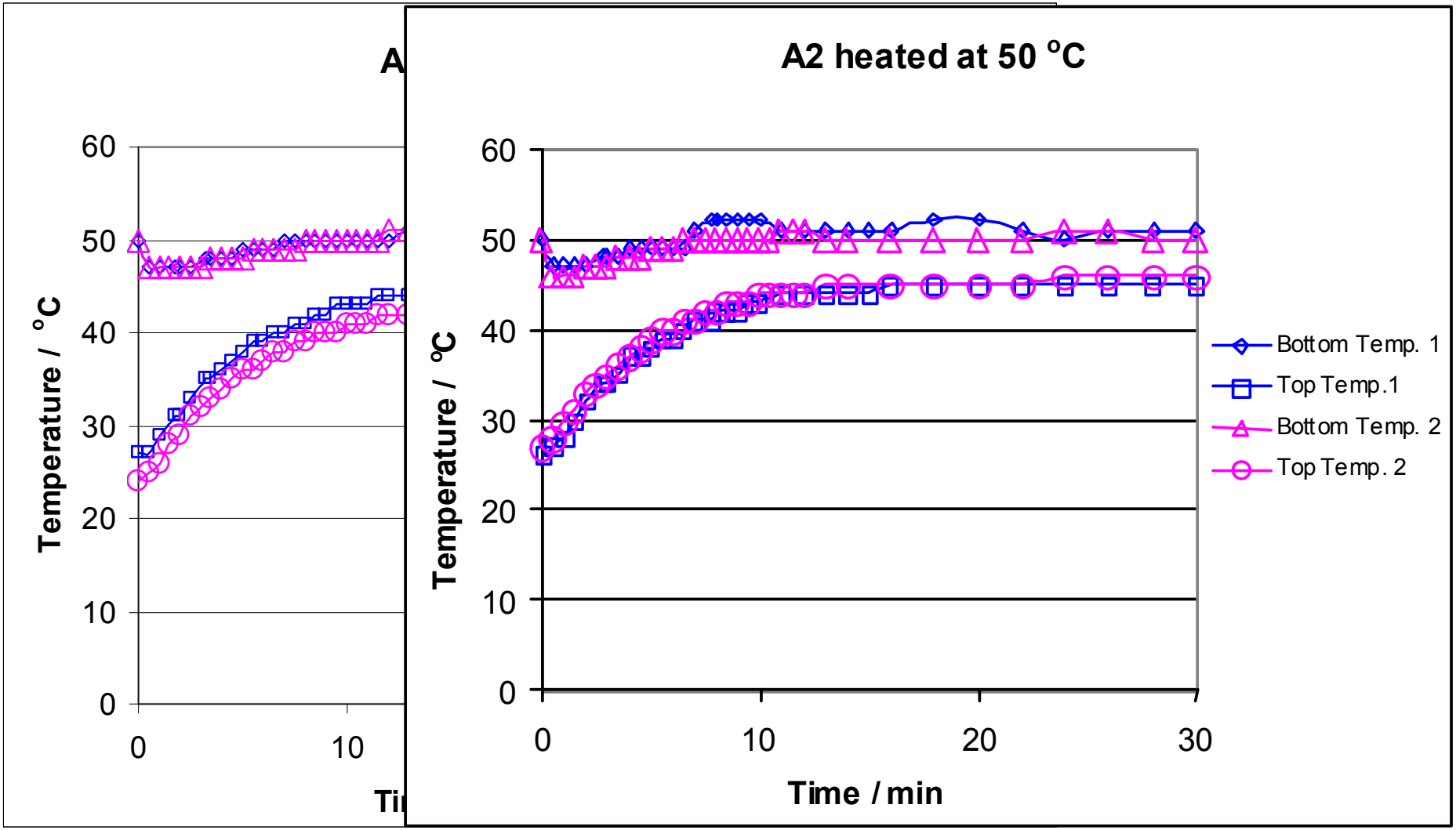

Differential analysis

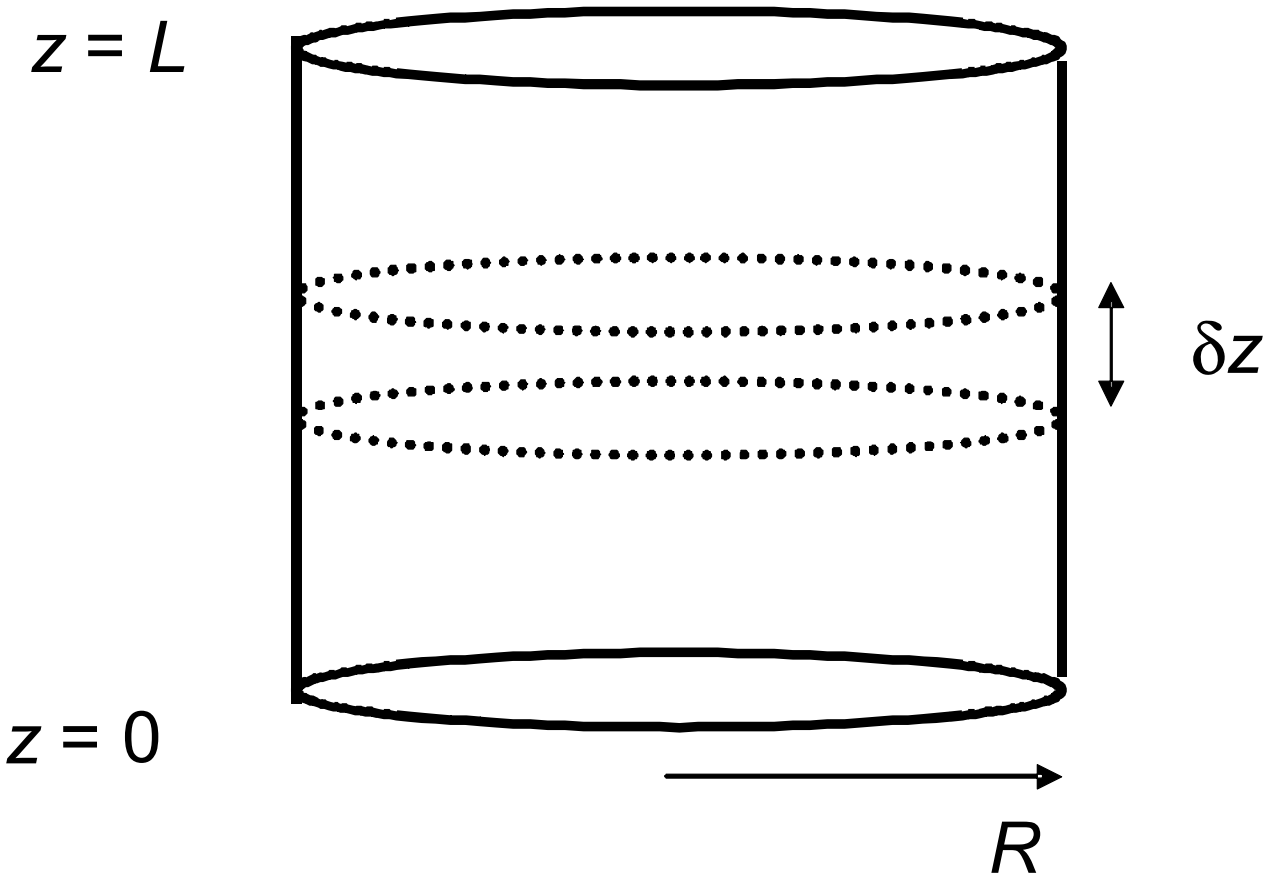

Theory

Rate of heat transfer along the axis of a cylinder:

Fourier's Law of heat conduction

$$\rho C_{\mathrm{p}} \frac{\partial T}{\partial t} = k \frac{\partial^2 T}{\partial z^2} - 2\frac{h}{R}(T - T_{\mathrm{a}})$$

ρ	density of the material
C_{p}	heat capacity
T	temperature of material at any position
T_{a}	of ambient air
k	thermal conductivity
h	heat transfer coefficient
R	radius of the cylinder.

Temperature at top using 2 different thermal transfer coefficients

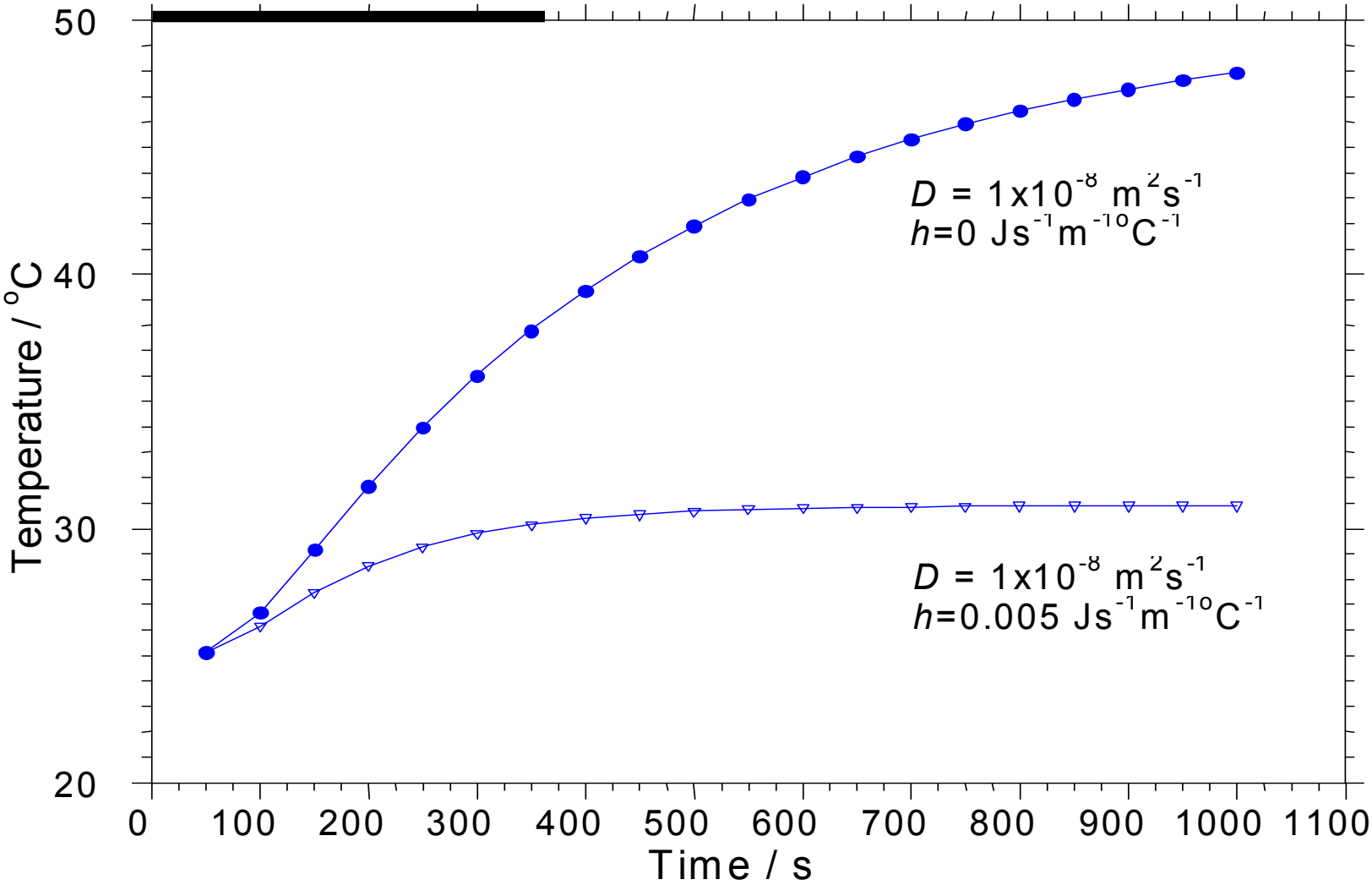

Temperature profile within sample

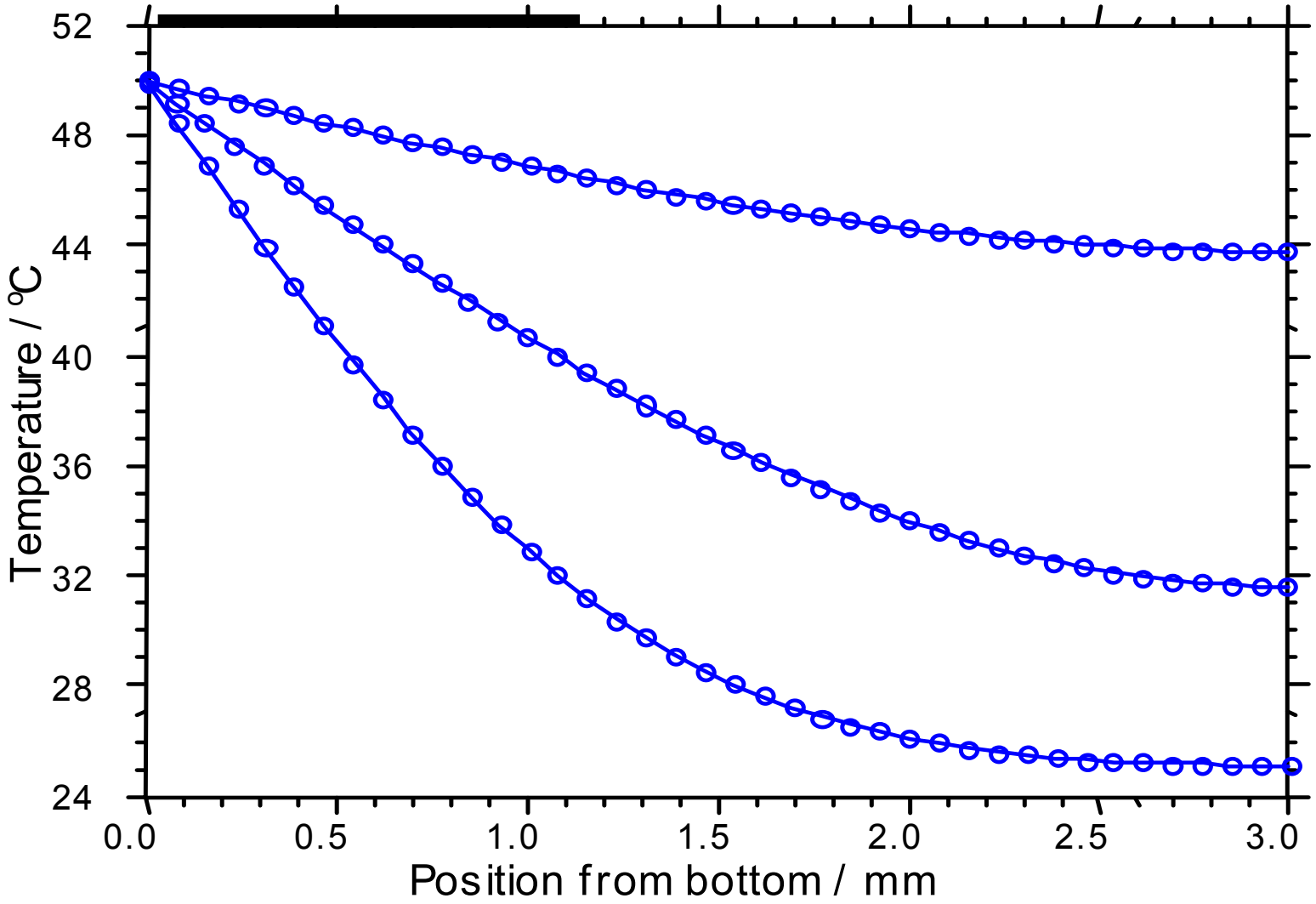

Example of match with experiment

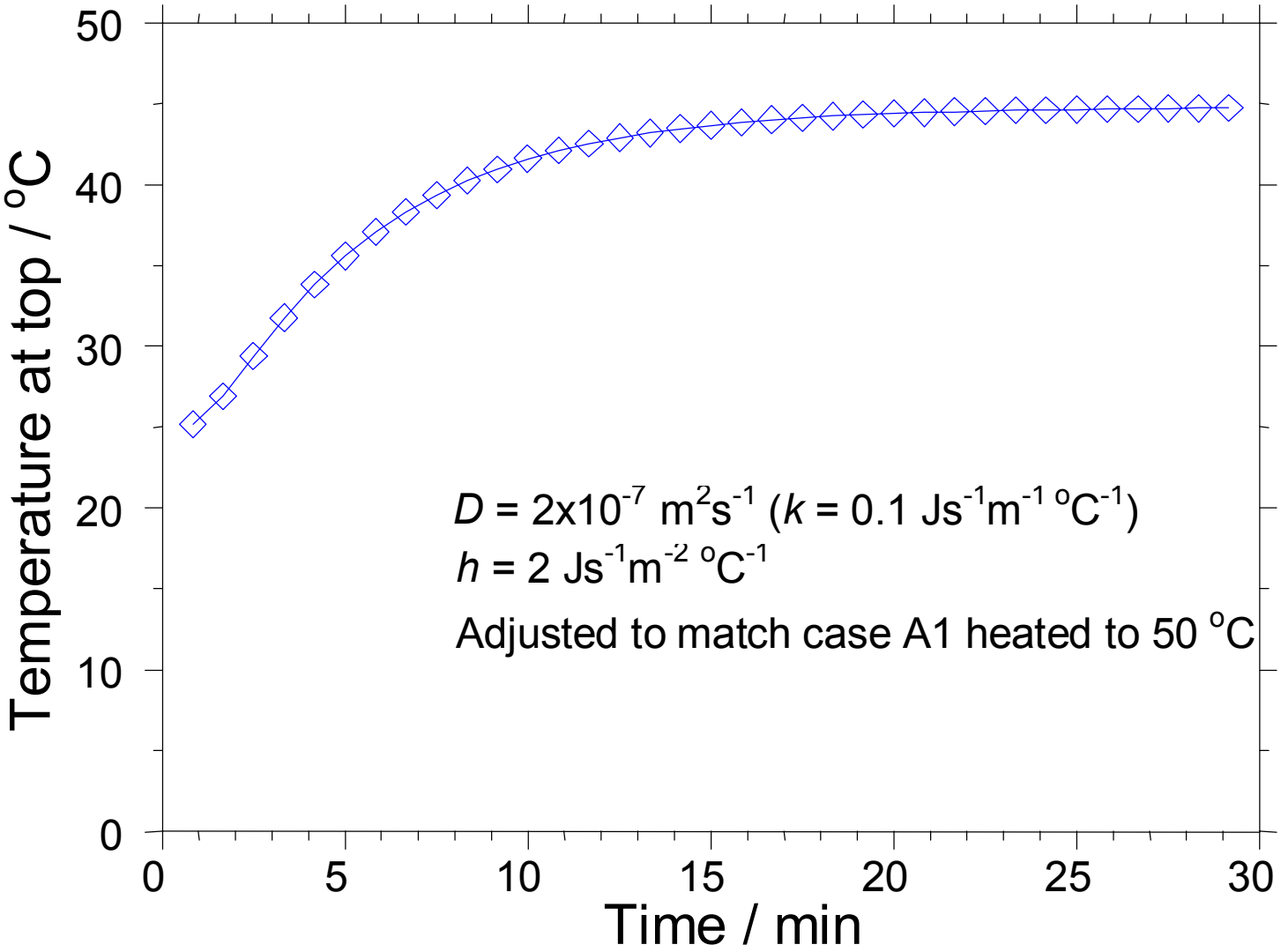

Results

	Diameter	Height	Porosity /%	Heat capacity	H Heat capacity	Thermal conductivity
	/mm	/mm	/ %	/cal $g^{-1}{}^{o}C^{-1}$	/J $kg^{-1}{}^{o}C^{-1}$	/$Js^{-1}m^{-1}{}^{o}C^{-1}$
A	29.20	12.71	47	0.13	543	**0.11**
B	38.86	12.22	30	0.14	585	**0.13**
C	36.92	12.93	38	0.12	501	**0.08**
D5	27.42	8.08	40	0.13	543	**0.24**

Interim conclusion 1

- **Differences are seen with sample D having greater thermal conductivity**

- **Is it due to structure?**

Pore structure by mercury intrusion porosimetry

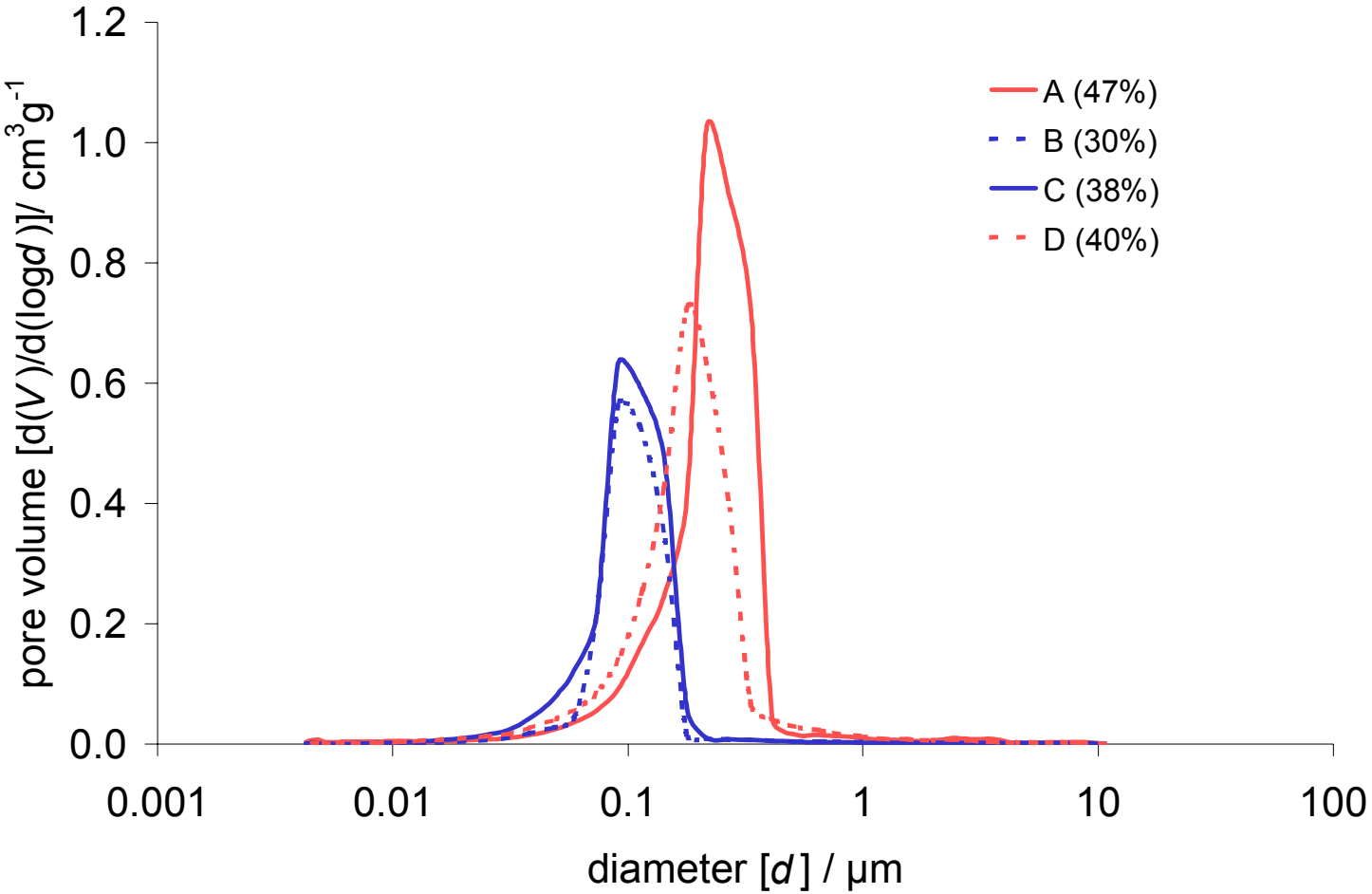

Example fit of modelled pore structure (sample C)

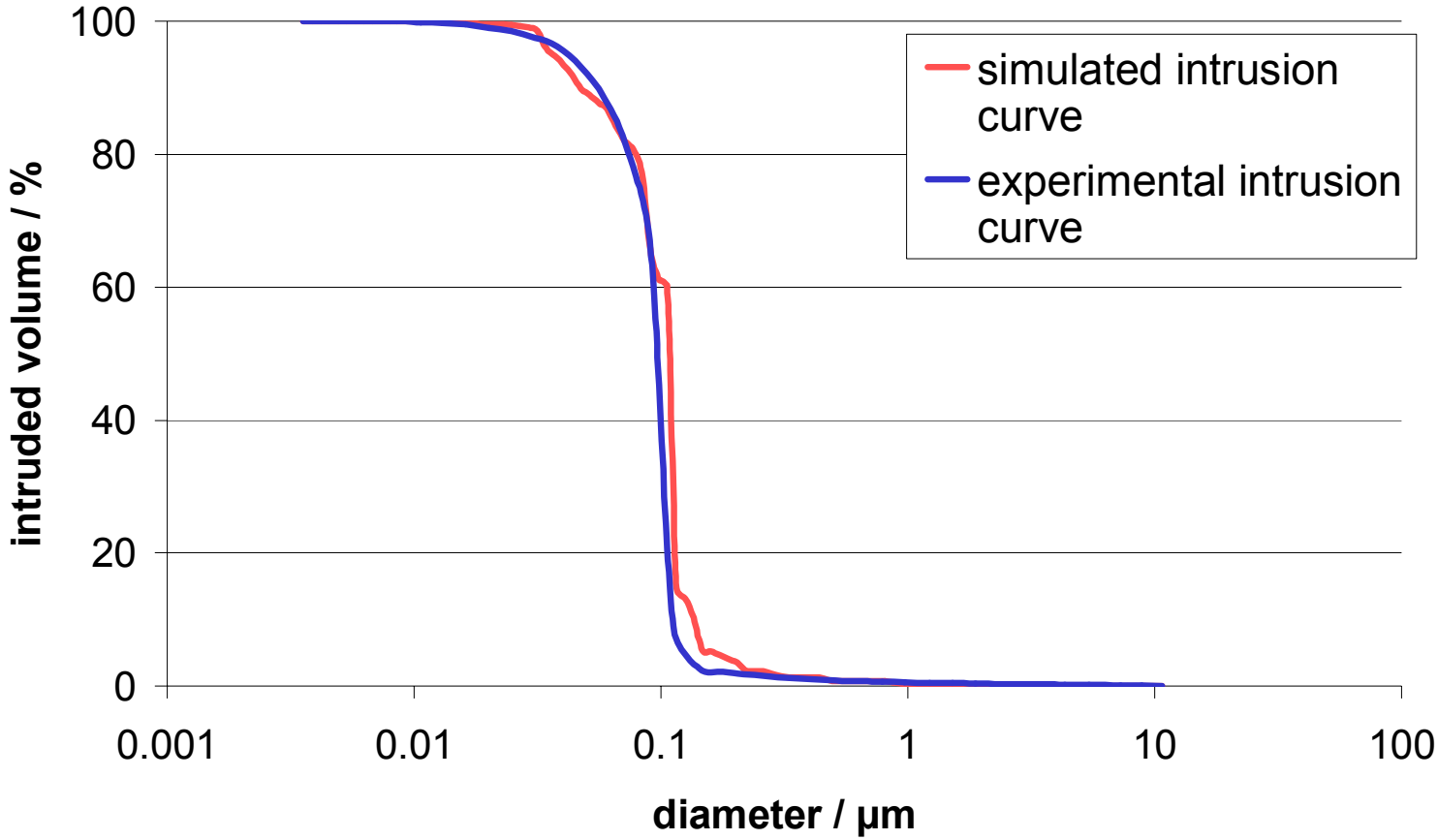

Pore network model (sample C)

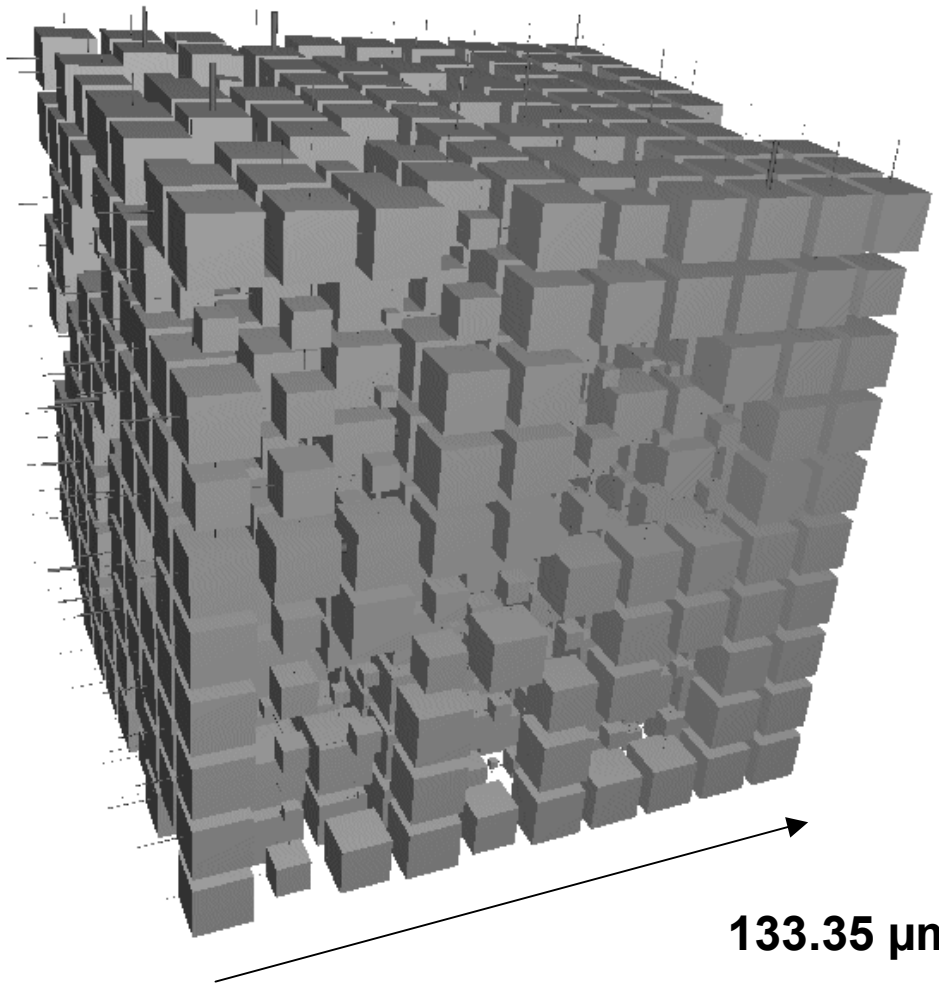

Pore-Cor is a software model by the Fluid and Environmental Modelling Group, University of Plymouth

Model network parameters

	min. diam / µm	max. diam / µm	throat skew	connectivity	pore skew	porosity / %	unit cell size / µm
A	0.004	10.69	1.60	4.56	115.58	47	135.1
B	0.004	10.69	2.49	5.31	77.56	30	144.3
C	0.004	10.69	2.49	5.31	77.56	38	133.4
D	0.004	10.69	2.00	5.00	200.00	40	143.1

Permeability gases and liquid

Darcy´s Law

$$\frac{\mathrm{d}V}{\mathrm{d}t} = k\frac{A\,\Delta P}{\eta\, l}$$

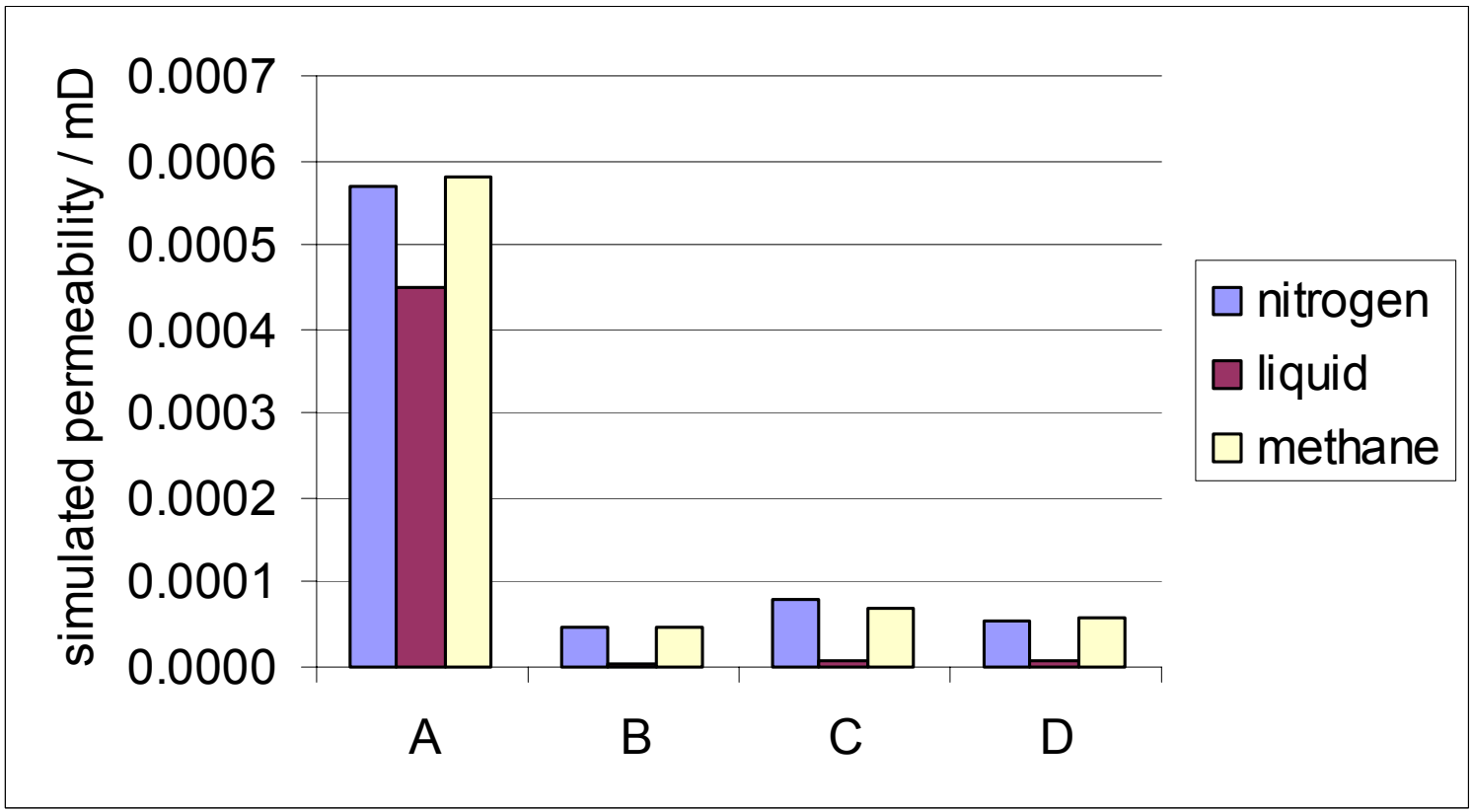

Interim conclusion 2

- **Porosity does not correlate directly**
- **Connectivity is a necessary but not sufficient condition for thermal conductivity**
- **Permeability, related to connectivity, and does not correlate with thermal conductivity**

- ***We are dealing with a combination***
  - **material property and structure**

Heating rate prediction at 150 °C

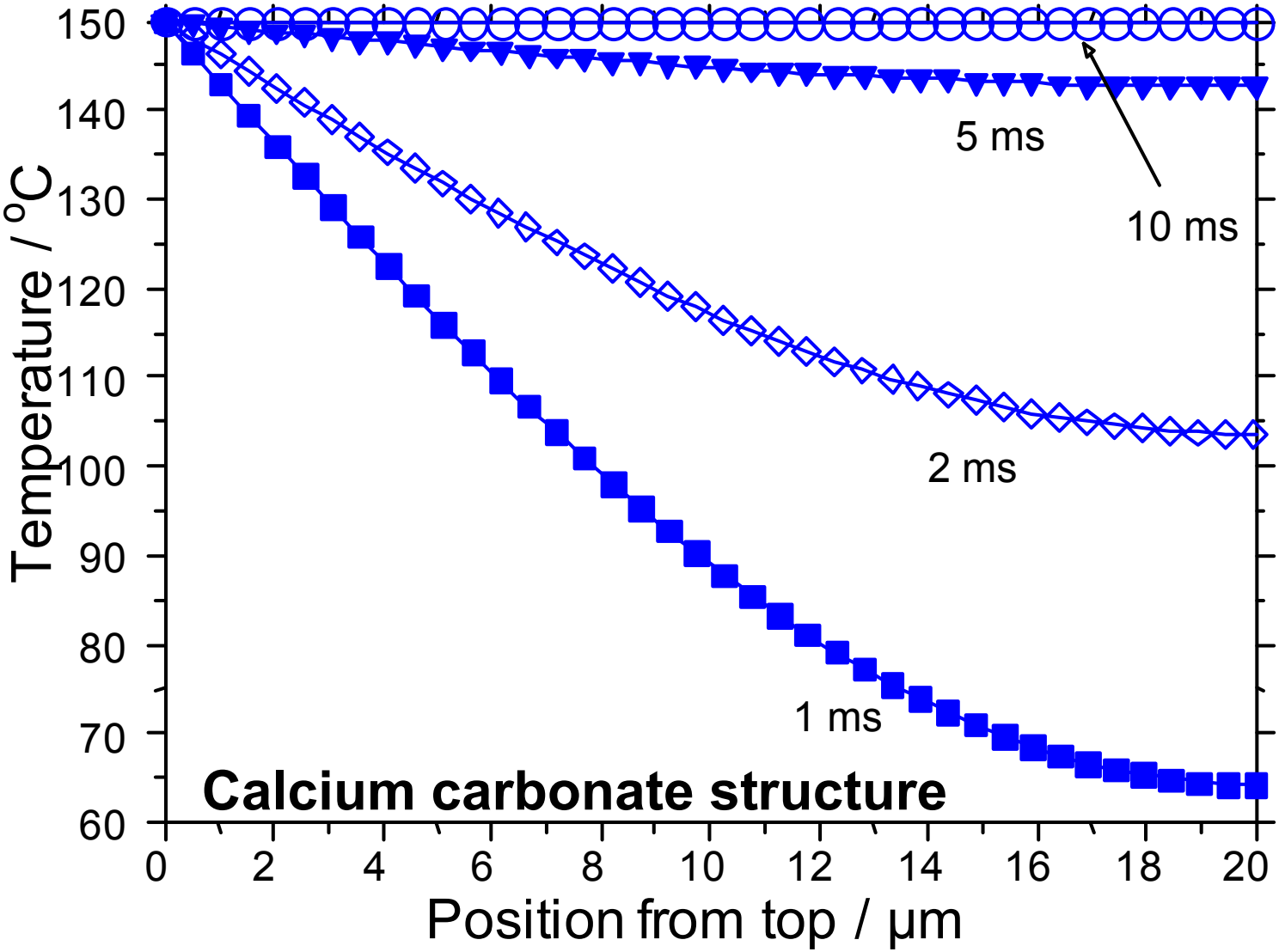

Heating rate prediction at 150 °C

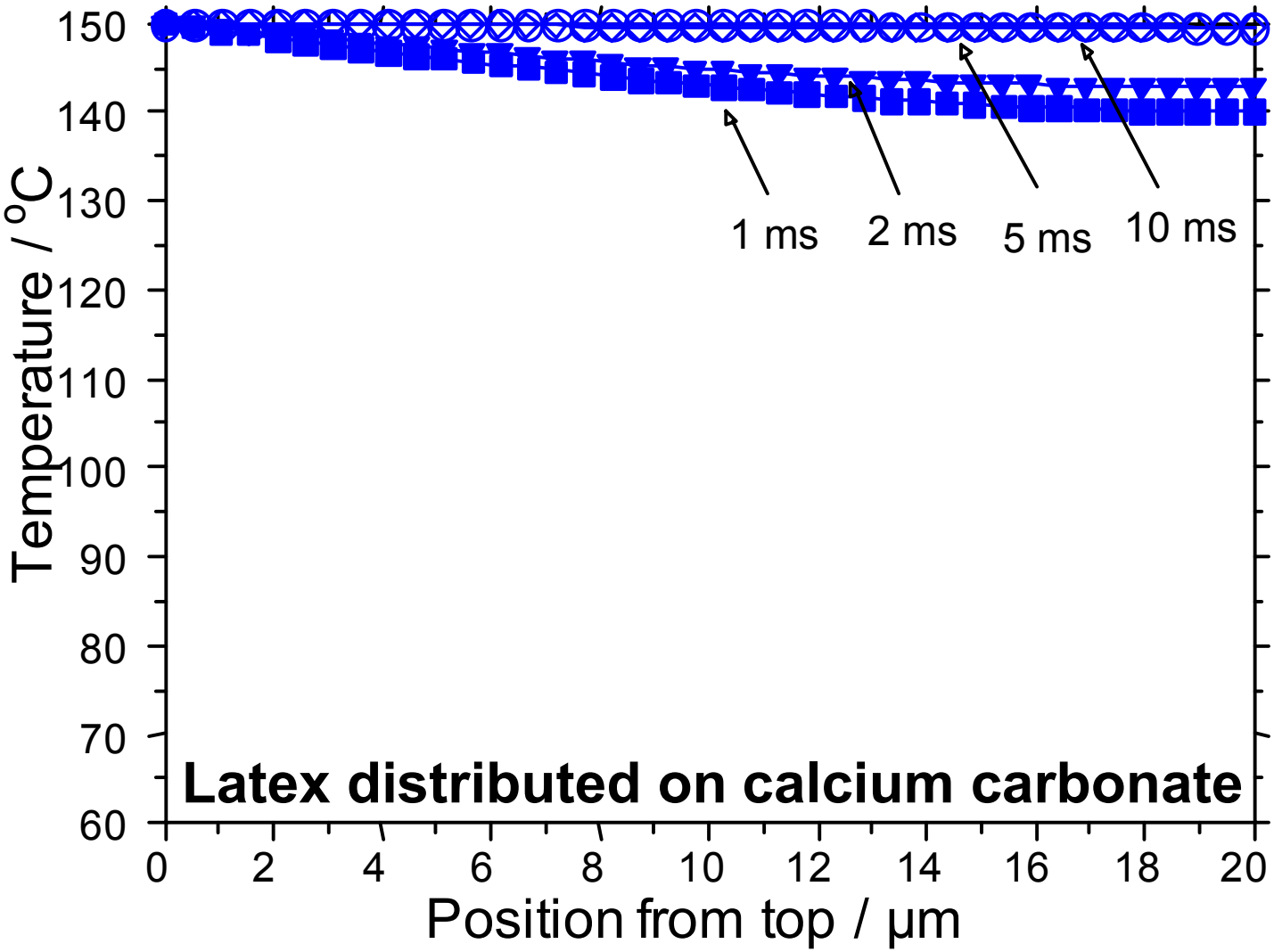

Summary of Conclusions

- **Thermal conductivity of coating structures can be measured using the tablet technique**
- **Modelling the thermal properties allows predicitons to be made for thin layers**
- **Thermal conductivity is a function of material distribution and structure (connectivity being necessary)**
  - **Material property dominates for typical structures**
  - **Latex/polymer distribution is the most dominant parameter in paper coatings**
    - **Can be used to control fusing properties**

Thanks to co-authors

Dr. Cathy J. Ridgway
Dr. J. Schölkopf
Omya Development AG

Prof. Douglas J. Bousfield
University of Maine

Omya